

# On the background correction of the Cornell fast rotation Fourier analysis

J. Fagin<sup>1</sup>, A. Chapelain<sup>1</sup>, D. Rubin<sup>1</sup>, and D. Seleznev<sup>1</sup>

<sup>1</sup>Cornell University

## Abstract

The muon frequency distribution is found by taking the cosine Fourier transformation of the fast rotation signal. The cosine Fourier transformation should begin at a time  $t_0$  when the centroid of the time profile of the muon beam first passes the detector. We want to start the Fourier transform at a later start time  $t_s$  in order to skip the beam-line positron contamination of the muon beam which continues for the first  $4 \mu s$  and possibly to skip scraping which lasts for the first  $30 \mu s$  of the fast rotation signal. The missing time between  $t_0$  and  $t_s$  of the cosine Fourier transformation must be accounted for. This missing time creates a background on the cosine Fourier transformation which must be removed. We fitted the background and then subtract it to recovered the complete frequency distribution.

The background can be fitted using different functions which are all equivalent for values of  $t_s$  of at least  $4 \mu s$ , enough to skip the positron contamination. The background can be fitted accurately for values of  $t_s$  up to  $25 \mu s$  for both Gaussian and asymmetric Monte Carlo fast rotation signals using some fit functions. For frequency distributions with higher statistics and less width, we would likely be able to fit the background all the way up to  $30 \mu s$  allowing us to skip all of scraping.

We also offer an alternative approach by first approximate the frequency distribution and then using the approximation to calculate the background. An iterative process can be used which self corrects the background allowing us to instead start with the cosine Fourier transformation as the approximate frequency distribution. These approaches work precisely for values of  $t_s$  of at least  $4 \mu s$  but falter when  $t_s$  is greater than  $8 \mu s$ .

## Contents

|          |   |           |
|----------|---|-----------|
| <b>1</b> | <b>Introduction</b>   | <b>2</b>  |
| <b>2</b> | <b>Analytic forms of the background of the cosine Fourier transform</b>         | <b>4</b>  |
| 2.1      | Dirac delta frequency distribution . . . . .                                    | 4         |
| 2.2      | Step function frequency distribution . . . . .                                  | 5         |
| 2.3      | Gaussian frequency distribution . . . . .                                       | 6         |
| 2.4      | Triangular frequency distribution . . . . .                                     | 8         |
| 2.5      | Discussion of other possible analytic forms . . . . .                           | 11        |
| <b>3</b> | <b>Analytic background comparisons of the cosine Fourier transform</b>          | <b>11</b> |
| 3.1      | Comparison of the delta, step, Gaussian, and triangular backgrounds . . . . .   | 11        |
| 3.2      | The background cancels the frequency distribution at late start times . . . . . | 12        |

|    |  |           |
|----|--|-----------|
| 31 | <b>4 Monte Carlo fitting with a Gaussian frequency distribution</b>    | <b>14</b> |
| 32 | 4.1 polynomial . . . . .   | 16        |
| 33 | 4.2 sinc . . . . .   | 17        |
| 34 | 4.3 Si . . . . .   | 19        |
| 35 | 4.4 erfi . . . . .   | 21        |
| 36 | 4.5 Triangular . . . . .   | 22        |
| 37 | <b>5 Monte Carlo fitting with an asymmetric frequency distribution</b> | <b>24</b> |
| 38 | 5.1 Fit comparison . . . . .   | 26        |
| 39 | 5.2 E-field comparison . . . . .                                       | 29        |
| 40 | <b>6 Conclusion of background fit method</b>                           | <b>30</b> |
| 41 | <b>7 Integral approach to the frequency background</b>                 | <b>30</b> |
| 42 | 7.1 Lifting the frequency distribution . . . . .                       | 30        |
| 43 | 7.2 Iteratively approximating the frequency . . . . .                  | 33        |
| 44 | <b>8 Conclusion of integration method</b>                              | <b>36</b> |
| 45 | <b>Appendices</b>  | <b>37</b> |
| 46 | <b>A When is <math>t_s</math> small?</b>                               | <b>37</b> |
| 47 | <b>B Approximating the step function to be a Gaussian</b>              | <b>37</b> |
| 48 | B.1 Gaussian frequency distribution . . . . .                          | 38        |
| 49 | B.2 Skewed Gaussian frequency distribution . . . . .                   | 40        |
| 50 | <b>C Approximating the step function to be a Dirac delta function</b>  | <b>44</b> |
| 51 | C.1 Spherical Bessel function . . . . .                                | 44        |
| 52 | C.2 sinc background approximation . . . . .                            | 45        |

## 53 1 Introduction

54 The goal of the fast rotation Fourier analysis is to calculate the E-field correction to  $\omega_a$  which is the precession  
55 frequency of the muon's spin about its momentum. The E-field correction is directly calculated from the  
56 radial distribution of the muons which is produced from the frequency distribution. To calculate the E-field  
57 correction, we must be able to extract the frequency distribution from the fast rotation signal to a high degree  
58 of accuracy [1].

59 The frequency distribution of the muons about the ring is obtained by doing a Fourier transformation of the  
60 fast rotation signal. The fast rotation signal is the change in the intensity of the muons as they go around the  
61 ring at a fixed location. since the frequency distribution of the muons is approximately even about its center,  
62 the frequency distribution is obtained by taking the real part of the Fourier transformation, which is the cosine  
63 Fourier transformation [2].

64 When taking the cosine Fourier transformation of the fast rotation signal, we must skip the first several  
65 microseconds of data because there is beam-line positron contamination of the muon beam which is gone by 4  
66  $\mu\text{s}$ . Figure 1 shows the beam-line positron contamination of the muon beam on the first first 4  $\mu\text{s}$  of the fast  
67 rotation signal for the Run-1 60-hour data set. The first 30  $\mu\text{s}$  of the fast rotation signal is afflicted by scraping  
68 which may affect the radial distribution of the muons, so ideally we also want the ability skip this as well.

69 The cosine Fourier transformation ideally begins at the time when the centroid of the time profile of the  
70 muon beam first passes the detector denoted as  $t_0$ . We must instead start the cosine Fourier transformation  
71 of the fast rotation signal not at  $t_0$  but instead a later start time  $t_s$  to skip the positron contamination and  
72 ideally scraping. To recover an accurate frequency distribution, the missing time in the cosine Fourier transform  
73 between  $t_0$  and  $t_s$  must be accounted for.

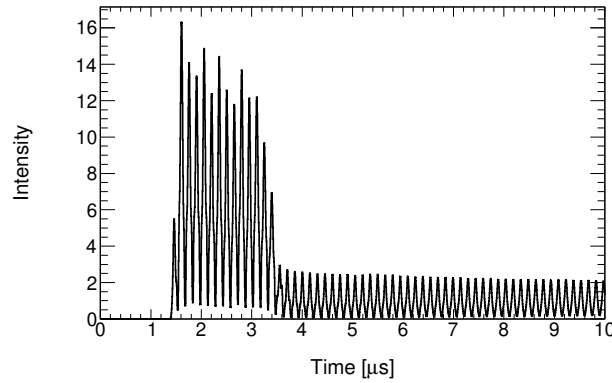


Figure 1: The first 10  $\mu\text{s}$  of the fast rotation signal is shown for Run-1 60-hour data set. The positron interference can be seen in the first 4  $\mu\text{s}$  of the signal.

74 For a fast rotation signal  $S(t)$ , the frequency distribution  $\tilde{S}(\omega)$  can be recovered via the cosine Fourier  
75 transform [2]:

$$\tilde{S}(\omega) = \sqrt{\frac{2}{\pi}} \int_{t_0}^{\infty} S(t) \cos \omega(t - t_0) dt = \sqrt{\frac{2}{\pi}} \int_{t_s}^{\infty} S(t) \cos \omega(t - t_0) dt + \sqrt{\frac{2}{\pi}} \int_{t_0}^{t_s} S(t) \cos \omega(t - t_0) dt. \quad (1)$$

76 The integral between  $t_0$  and  $t_s$  is the correction to the fast rotation signal denoted  $\Delta(\omega)$ . The correction is  
77 equal to the following equation where  $\omega^+ = 6.748$  MHz and  $\omega^- = 6.663$  MHz are the bounds of the collimator  
78 aperture [2]:

$$\Delta(\omega) = \sqrt{\frac{2}{\pi}} \int_{t_0}^{t_s} S(t) \cos \omega(t - t_0) dt \approx \frac{1}{\pi} \int_{\omega^-}^{\omega^+} \tilde{S}(\omega') \frac{\sin[(\omega - \omega')(t_s - t_0)]}{\omega - \omega'} d\omega'. \quad (2)$$

79 We add the correction to the cosine Fourier transformation in order to recover the complete frequency dis-  
80 tribution. We do this by fitting for the background to the cosine Fourier transformation which is the negative of  
81 the correction. Then we subtract the background from the cosine Fourier transformation yielding the complete  
82 frequency distribution.

83

84 **Important note:** The equation (2) above and all the other equations in this note use angular frequencies  
85  $\omega$ , however all figures are shown using frequency  $f$  where  $\omega = 2\pi f$ . Using angular frequency makes calculations

86 clearer, but to get physically meaningful figures all angular frequencies must be converted to regular frequencies  
 87 by dividing by  $2\pi$ .

## 88 **2 Analytic forms of the background of the cosine Fourier transform**

89 The goal of this work is to derive general analytical forms of the cosine Fourier transform background in  
 90 order to be able to fit for it and therefore correct for it for simulated and real data. Analytical frequency  
 91 distributions with increasing complexity and realism will be plugged into equation (2). The analytical form of  
 92 the cosine Fourier transform in the real data is not known but a general enough background form will be a  
 93 good approximation.

### 94 **2.1 Dirac delta frequency distribution**

95 For an arbitrary frequency distribution  $\tilde{S}(\omega)$  confined within the collimator aperture at  $\omega^-$  and  $\omega^+$ , we know the  
 96 form of the correction to the cosine Fourier transformation of the fast rotation signal is given by the following  
 97 equation:

$$\Delta(\omega) = \frac{1}{\pi} \int_{\omega^-}^{\omega^+} \tilde{S}(\omega') \frac{\sin[(\omega - \omega')(t_s - t_0)]}{\omega - \omega'} d\omega'. \quad (3)$$

98 We will first assume that the frequency distribution is a Dirac delta function centered at a frequency  $\omega_0$ :

$$\tilde{S}(\omega) = \delta(\omega - \omega_0). \quad (4)$$

99 We start with a Dirac delta function because it is the simplest function to integrate and only has a single  
 100 defining parameter which is its center. We plug the delta function ansatz into equation (3):

$$\Delta(\omega) = \frac{1}{\pi} \int_{\omega^-}^{\omega^+} \delta(\omega' - \omega_0) \frac{\sin[(\omega - \omega')(t_s - t_0)]}{\omega - \omega'} d\omega' = \frac{1}{\pi} \frac{\sin[(\omega - \omega_0)(t_s - t_0)]}{(\omega - \omega_0)}. \quad (5)$$

101 The background in equation (6) takes the form of a sinc function since:

$$\Delta(\omega) = \frac{(t_s - t_0)}{\pi} \text{sinc}[(\omega - \omega_0)(t_s - t_0)]. \quad (6)$$

102 We show in figure 2 the background for a Dirac delta function centered at the magic frequency with different  
 103 start times. The magic frequency is at 6.705 MHz. The input frequency distribution is the same Dirac delta  
 104 function each time, but the background changes with  $t_s$ .

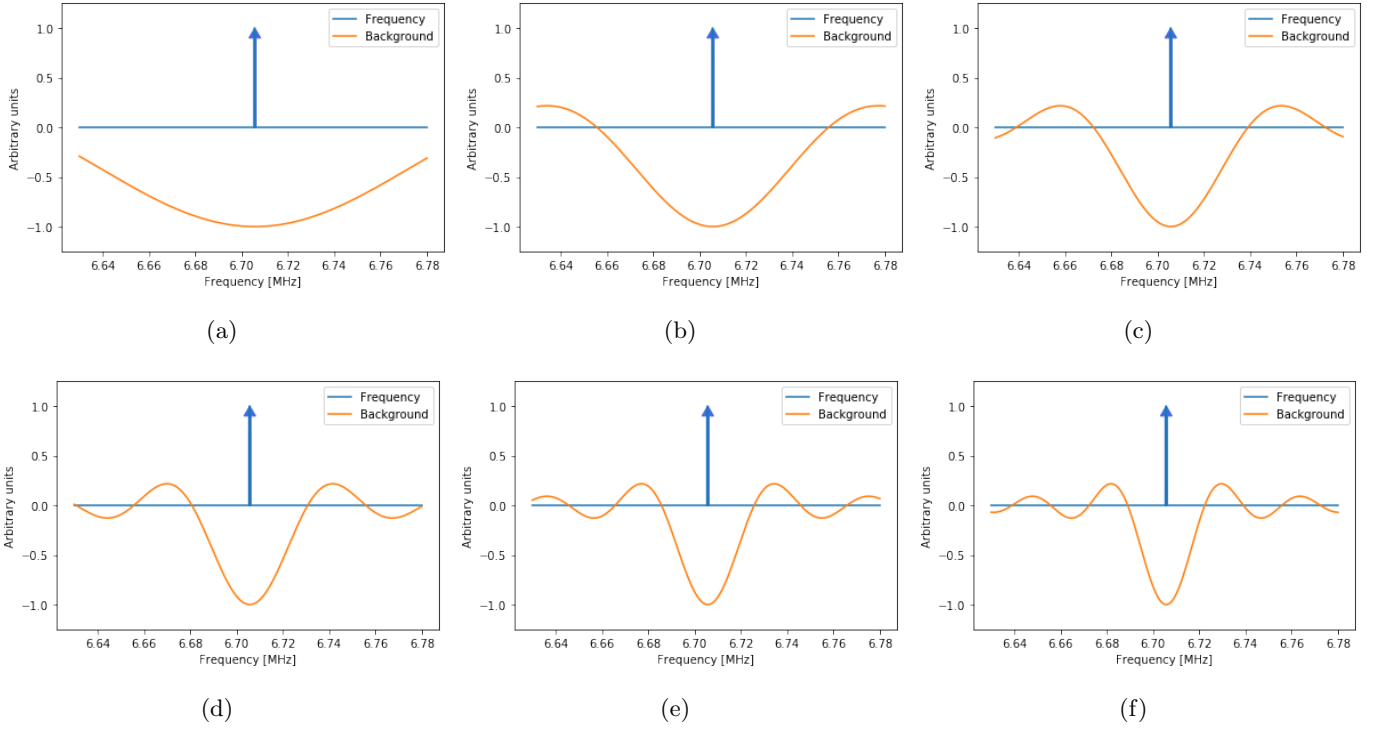


Figure 2: Background with  $t_0 = 0 \mu\text{s}$  and different values of  $t_s$  for a Dirac delta frequency distribution centered at the magic frequency. Six start times are shown: (a)  $5 \mu\text{s}$ , (b)  $10 \mu\text{s}$ , (c)  $15 \mu\text{s}$ , (d)  $20 \mu\text{s}$ , (e)  $25 \mu\text{s}$ , (f)  $30 \mu\text{s}$ .

## 105 2.2 Step function frequency distribution

106 The work done in the previous section assumed a Dirac delta frequency distribution. We can make a similar  
 107 derivation using a step function frequency distribution. We choose to use a step function because we are still  
 108 able to integrate it into equation (3) and it is a more realistic frequency distribution than a delta function since  
 109 the muon beam must have some spread around the ring.

110 The step function frequency distribution is defined between  $\omega_1$  and  $\omega_2$  where  $\omega_1$  and  $\omega_2$  are within the  
 111 bound of the collimator aperture and  $\omega_2 > \omega_1$ . Then we have a normalized frequency distribution as follows:

$$\tilde{S}(\omega) = \frac{1}{\omega_2 - \omega_1} \begin{cases} 1 & \omega_1 \leq \omega \leq \omega_2 \\ 0 & \text{else} \end{cases} \quad (7)$$

112 When we plug this directly into our equation for the background correction (3):

$$\Delta(\omega) = \frac{1}{\pi(\omega_2 - \omega_1)} \int_{\omega_1}^{\omega_2} \frac{\sin[(\omega - \omega')(t_s - t_0)]}{\omega - \omega'} d\omega' = \frac{1}{\pi(\omega_2 - \omega_1)} [\text{Si}((\omega - \omega_1)(t_s - t_0)) - \text{Si}((\omega - \omega_2)(t_s - t_0))], \quad (8)$$

113 where the Si function is defined as:

$$\text{Si}(x) = \int_0^x \frac{\sin(y)}{y} dy. \quad (9)$$

114 Using a step function frequency distribution is a large improvement from the Dirac delta function since we  
 115 can enclose any frequency distribution within a step function as a rough approximation for the correction to

116 the cosine Fourier transformation. The Dirac delta function only had a single characteristic parameter which  
 117 was its center. The step function frequency distribution has two characteristic parameters corresponding to  
 118 each bound of the step function. This additional parameter is an extra degree of freedom when fitting the  
 119 background which makes the fit work for much larger values of  $t_s$ . Figure 3 shows the background for a step  
 120 function centered at the magic frequency with a width of 10 kHz.

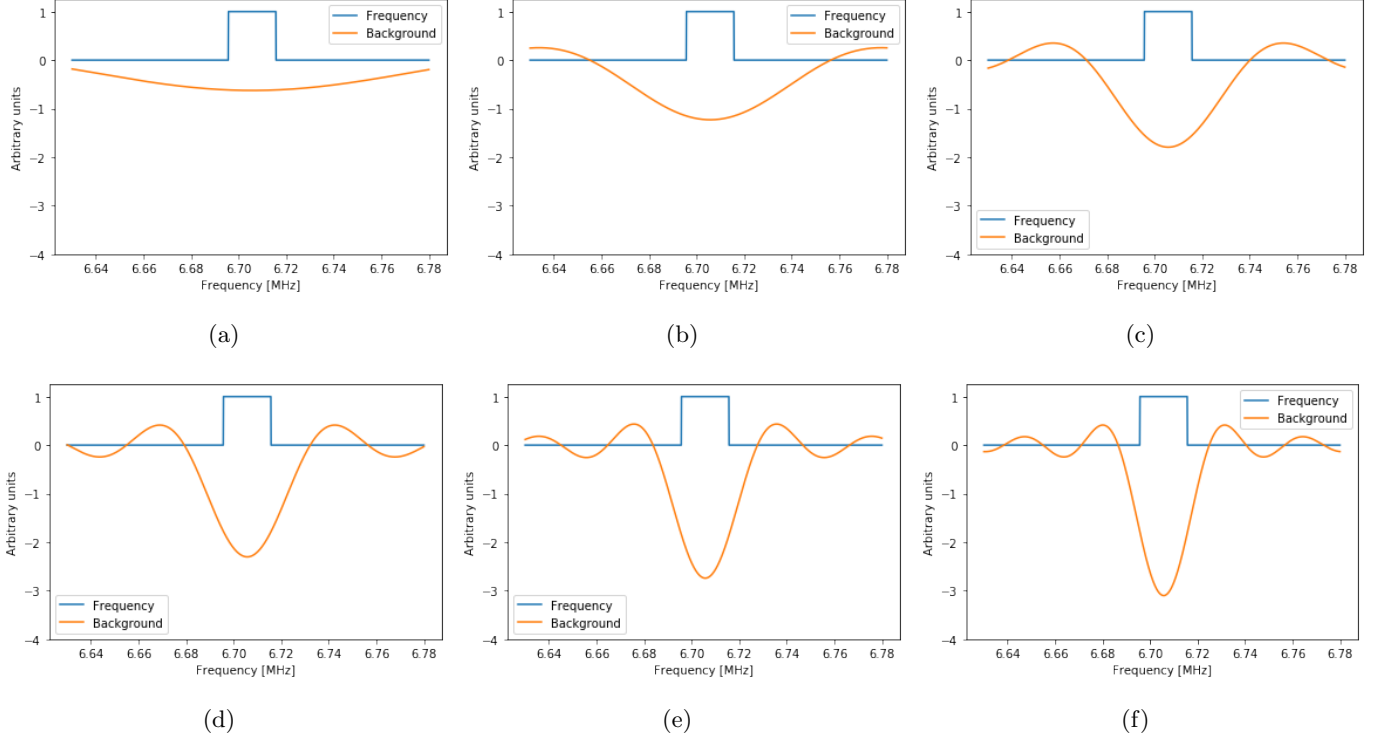


Figure 3: Background with  $t_0 = 0 \mu s$  and different values of  $t_s$  for a step function frequency distribution centered at the magic frequency and a width of  $\pm 10$  kHz. Six start times are shown: (a)  $5 \mu s$ , (b)  $10 \mu s$ , (c)  $15 \mu s$ , (d)  $20 \mu s$ , (e)  $25 \mu s$ , (f)  $30 \mu s$ .

### 121 2.3 Gaussian frequency distribution

122 We now consider a Gaussian frequency distribution since it is more realistic than the step function because the  
 123 muon beam for real data is smooth without the jagged corners that a step function has. We assume a Gaussian  
 124 frequency distribution centered at the magic frequency  $\omega_0$  with standard deviation  $\sigma$ :

$$\tilde{S}(\omega) = \frac{1}{\sqrt{2\pi}\sigma} e^{-\frac{(\omega-\omega_0)^2}{2\sigma^2}}. \quad (10)$$

125 We then plug the Gaussian frequency distribution directly into equation (3):

$$\Delta(\omega) = \frac{1}{\pi} \int_{\omega^-}^{\omega^+} \frac{1}{\sqrt{2\pi}\sigma} e^{-\frac{(\omega'-\omega_0)^2}{2\sigma^2}} \frac{\sin[(\omega - \omega')(t_s - t_0)]}{\omega - \omega'} d\omega'. \quad (11)$$

126 Physical frequency distributions must be confined within the collimator aperture since the muon beam must  
 127 exist within the ring. We assume a Gaussian frequency distribution whose full 5-standard-deviation width is  
 128 contained within the collimator aperture. Therefore, we evaluate the integral with arbitrarily large bounds

129 since the Gaussian will be close to zero outside the physical frequency range. This is necessary so that the  
 130 integral can be evaluated analytically.

$$\Delta(\omega) = \frac{1}{\sqrt{2\pi^3\sigma^2}} \int_{-\infty}^{+\infty} e^{-\frac{(\omega' - \omega_0)^2}{2\sigma^2}} \frac{\sin[(\omega - \omega')(t_s - t_0)]}{\omega - \omega'} d\omega', \quad (12)$$

131 and now we can evaluate the integral:

$$\begin{aligned} \Delta(\omega) &= \frac{1}{\sqrt{2\pi^3\sigma^2}} \int_0^{t_s - t_0} dt \int_{-\infty}^{+\infty} e^{-\frac{(\omega' - \omega_0)^2}{2\sigma^2}} \cos(\omega - \omega') t d\omega' \\ &= \frac{1}{\sqrt{2\pi^3\sigma^2}} \int_0^{t_s - t_0} dt \operatorname{Re} \left\{ \int_{-\infty}^{+\infty} e^{-\frac{(\omega' - \omega_0)^2}{2\sigma^2} + i(\omega - \omega')t} d\omega' \right\} \\ &= \frac{1}{\sqrt{2\pi^3\sigma^2}} \int_0^{t_s - t_0} dt \operatorname{Re} \left\{ \int_{-\infty}^{+\infty} e^{-\frac{\omega'^2}{2\sigma^2} + (\frac{\omega_0}{\sigma^2} - it)\omega' + i\omega t - \frac{\omega_0^2}{2\sigma^2}} d\omega' \right\}. \end{aligned} \quad (13)$$

132 The inner integral can be evaluated since it is a standard Gaussian integral of a degree two polynomial. It  
 133 is solved by completing the square as follows:

$$\begin{aligned} \Delta(\omega) &= \frac{1}{\sqrt{2\pi^3\sigma^2}} \int_0^{t_s - t_0} dt \operatorname{Re} \left\{ \sqrt{2\pi\sigma^2} e^{\frac{\sigma^2}{2} (\frac{\omega_0}{\sigma^2} - it)^2 + i\omega t - \frac{\omega_0^2}{2\sigma^2}} \right\} = \frac{1}{\pi} e^{-\frac{\omega_0^2}{2\sigma^2}} \operatorname{Re} \left\{ \int_0^{t_s - t_0} e^{\frac{\sigma^2}{2} (\frac{\omega_0}{\sigma^2} - it)^2 + i\omega t} dt \right\} \\ &= \frac{1}{\pi} e^{-\frac{\omega_0^2}{2\sigma^2}} \operatorname{Re} \left\{ i \sqrt{\frac{\pi}{2\sigma^2}} e^{-\frac{\omega_0\omega}{\sigma^2} - \frac{\omega^2}{2\sigma}} \left[ \operatorname{erfi} \left( \frac{\omega - \omega_0}{\sqrt{2\sigma^2}} \right) - \operatorname{erfi} \left( \frac{\omega - \omega_0 + i\sigma^2(t_s - t_0)}{\sqrt{2\sigma^2}} \right) \right] \right\} \\ &= \frac{1}{\sqrt{2\pi\sigma^2}} e^{-\frac{(\omega - \omega_0)^2}{2\sigma^2}} \operatorname{Re} \left\{ i \left[ \operatorname{erfi} \left( \frac{\omega - \omega_0}{\sqrt{2\sigma^2}} \right) - \operatorname{erfi} \left( \frac{\omega - \omega_0 + i\sigma^2(t_s - t_0)}{\sqrt{2\sigma^2}} \right) \right] \right\}, \end{aligned} \quad (14)$$

134 where the error function,  $\operatorname{erf}(x)$ , is defined by the following equation:

$$\operatorname{erf}(x) = \frac{2}{\sqrt{\pi}} \int_0^x e^{-y^2} dy. \quad (15)$$

135 The imaginary error function is defined such that:  $\operatorname{erfi}(x) = -i \operatorname{erf}(ix)$ . The first  $\operatorname{erfi}$  function in equation  
 136 (14) can be eliminated because  $i \operatorname{erfi} \left( \frac{\omega - \omega_0}{\sqrt{2\sigma^2}} \right)$  will always be imaginary so its real part is zero so:

$$\begin{aligned} \Delta(\omega) &= \frac{1}{\sqrt{2\pi\sigma^2}} e^{-\frac{(\omega - \omega_0)^2}{2\sigma^2}} \operatorname{Re} \left\{ -i \operatorname{erfi} \left( \frac{\omega - \omega_0 + i\sigma^2(t_s - t_0)}{\sqrt{2\sigma^2}} \right) \right\} \\ &= \frac{1}{\sqrt{2\pi\sigma^2}} e^{-\frac{(\omega - \omega_0)^2}{2\sigma^2}} \operatorname{Im} \left\{ \operatorname{erfi} \left( \frac{\omega - \omega_0 + i\sigma^2(t_s - t_0)}{\sqrt{2\sigma^2}} \right) \right\}. \end{aligned} \quad (16)$$

137 The form of the correction we derived in equation (16) is proportional to the original Gaussian frequency  
 138 distribution such that:

$$\Delta(\omega) = \tilde{S}(\omega) \operatorname{Im} \left\{ \operatorname{erfi} \left( \frac{\omega - \omega_0 + i\sigma^2(t_s - t_0)}{\sqrt{2\sigma^2}} \right) \right\}. \quad (17)$$

139 Similarly to the step function, the Gaussian frequency distribution has two characteristic parameters corre-  
 140 sponding to the mean and standard deviation of the Gaussian. The Gaussian and step function therefore have  
 141 the same number of degrees of freedom, however a Gaussian frequency distribution is a better representative

142 of real data. Featured in figure 4 is the background calculated using equation (16) with different values of  $t_s$   
 143 for a frequency distribution centered at the magic frequency with a standard deviation of 5 kHz.

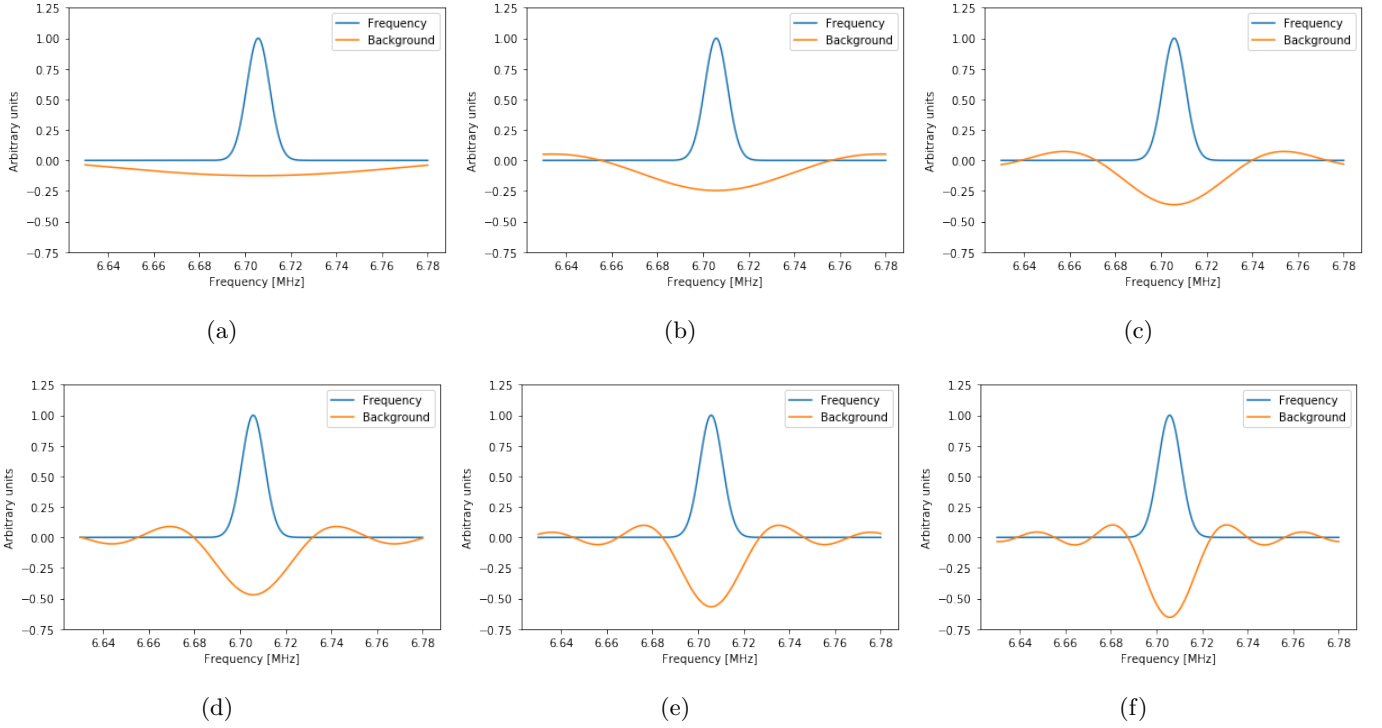


Figure 4: Background with  $t_0 = 0 \mu s$  and different values of  $t_s$  for a Gaussian frequency distribution centered at the magic frequency and a standard deviation of 5 kHz. Six start times are shown: (a)  $5 \mu s$ , (b)  $10 \mu s$ , (c)  $15 \mu s$ , (d)  $20 \mu s$ , (e)  $25 \mu s$ , (f)  $30 \mu s$ .

## 144 2.4 Triangular frequency distribution

145 We can also derive the form of the correction to the cosine Fourier transform by assuming a triangular frequency  
 146 distribution. We want to do this because a triangular frequency distribution is very similar to a Gaussian  
 147 frequency distribution since we can approximately contain a triangle within a Gaussian. The benefit of the  
 148 triangle is that since it does not have to be symmetric about its center, the analytic form of the correction  
 149 incorporates asymmetries in the frequency distribution.

150 We assume the triangle frequency distribution to be zero outside a range of  $\omega_1$  and  $\omega_2$  where  $\omega_1$  and  $\omega_2$   
 151 are within the bound of the collimator aperture, and the center of the triangle  $\omega_0$  is between them such that  
 152  $\omega_1 \leq \omega_0 \leq \omega_2$ . Then we have a normalized triangular frequency distribution of the following form:

$$\tilde{S}(\omega) = \frac{1}{2(\omega_2 - \omega_1)} \begin{cases} \frac{\omega - \omega_1}{\omega_0 - \omega_1} & \omega_1 \leq \omega \leq \omega_0 \\ \frac{\omega_2 - \omega}{\omega_2 - \omega_0} & \omega_0 < \omega \leq \omega_2 \\ 0 & \text{else} \end{cases} \quad (18)$$

153 We then plug the triangle frequency distribution (18) directly into our equation (3) for the background:

$$\begin{aligned}
\Delta(\omega) &= \frac{1}{\pi} \int_{\omega^-}^{\omega^+} \tilde{S}(\omega') \frac{\sin[(\omega - \omega')(t_s - t_0)]}{\omega - \omega'} d\omega' \\
&= \frac{1}{2\pi(\omega_2 - \omega_1)} \left[ \int_{\omega_1}^{\omega_0} \frac{\omega' - \omega_1}{\omega_0 - \omega_1} \frac{\sin[(\omega - \omega')(t_s - t_0)]}{\omega - \omega'} d\omega' + \int_{\omega_0}^{\omega_2} \frac{\omega_2 - \omega'}{\omega_2 - \omega_0} \frac{\sin[(\omega - \omega')(t_s - t_0)]}{\omega - \omega'} d\omega' \right] \\
&= \frac{1}{2\pi(\omega_2 - \omega_1)} \left[ \frac{\omega - \omega_1}{\omega_0 - \omega_1} [\text{Si}((\omega - \omega_1)(t_s - t_0)) - \text{Si}((\omega - \omega_0)(t_s - t_0))] + \frac{\cos((\omega - \omega_1)(t_s - t_0)) - \cos((\omega - \omega_0)(t_s - t_0))}{(\omega_0 - \omega_1)(t_s - t_0)} \right. \\
&\quad \left. + \frac{\omega_2 - \omega}{\omega_0 - \omega_2} [\text{Si}((\omega - \omega_1)(t_s - t_0)) - \text{Si}((\omega - \omega_0)(t_s - t_0))] - \frac{\cos((\omega - \omega_2)(t_s - t_0)) - \cos((\omega - \omega_0)(t_s - t_0))}{(\omega_0 - \omega_2)(t_s - t_0)} \right].
\end{aligned} \tag{19}$$

154 The triangle frequency distribution has three characteristic parameters instead of the two which the step  
155 function and Gaussian frequency distributions have. These parameters correspond to the bounds of the triangle  
156 and its center. The extra parameter gives an additional degree of freedom to the background fit which is able to  
157 incorporate the asymmetry of frequency distributions. This makes the triangle frequency distribution general  
158 enough to approximate a frequency distribution similar to real data.

159 Figure 5 shows the background for a triangular frequency distribution centered at the magic frequency with  
160 a width of 10 kHz. We can see that the form of the background looks almost identical to the Gaussian or step  
161 function backgrounds.

162 In figure 6 we show the background for a triangle frequency distribution centered at the magic frequency  
163 with a left bound of -10 kHz and a right bound of +30 kHz from its center. For values of  $t_s$  of 20  $\mu$ s and less,  
164 the background remains mostly symmetric about its center. When  $t_s$  becomes large, however, the background  
165 does not obey this symmetry but instead skews to the right. This is why the step function, Gaussian, and  
166 triangle frequency distributions can be fitted to the background for an asymmetric frequency distribution for  
167 approximately 20  $\mu$ s, but past this point only the triangular frequency background is able to include the  
168 asymmetry.

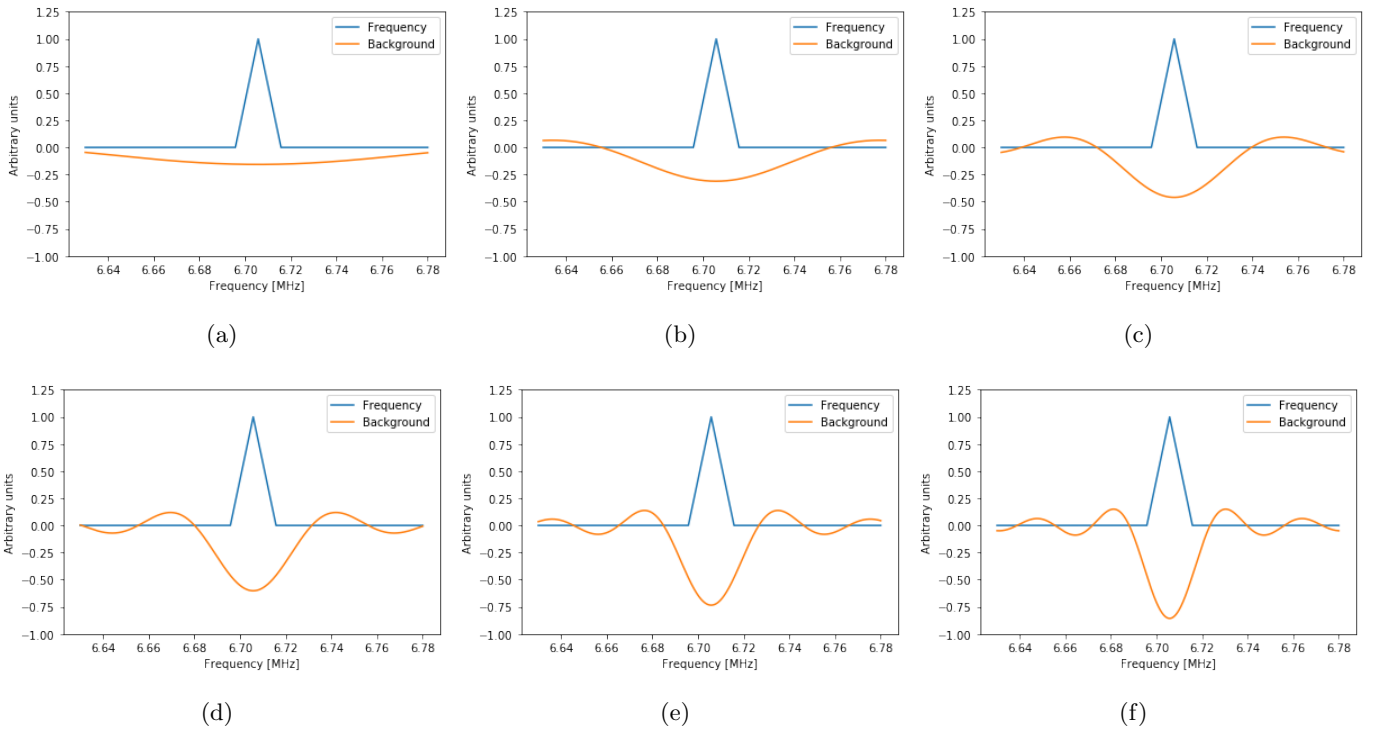


Figure 5: Background with  $t_0 = 0 \mu\text{s}$  and different values of  $t_s$  for a triangular frequency distribution centered at the magic frequency and bound 10 kHz from the center. Six start times are shown: (a)  $5 \mu\text{s}$ , (b)  $10 \mu\text{s}$ , (c)  $15 \mu\text{s}$ , (d)  $20 \mu\text{s}$ , (e)  $25 \mu\text{s}$ , (f)  $30 \mu\text{s}$

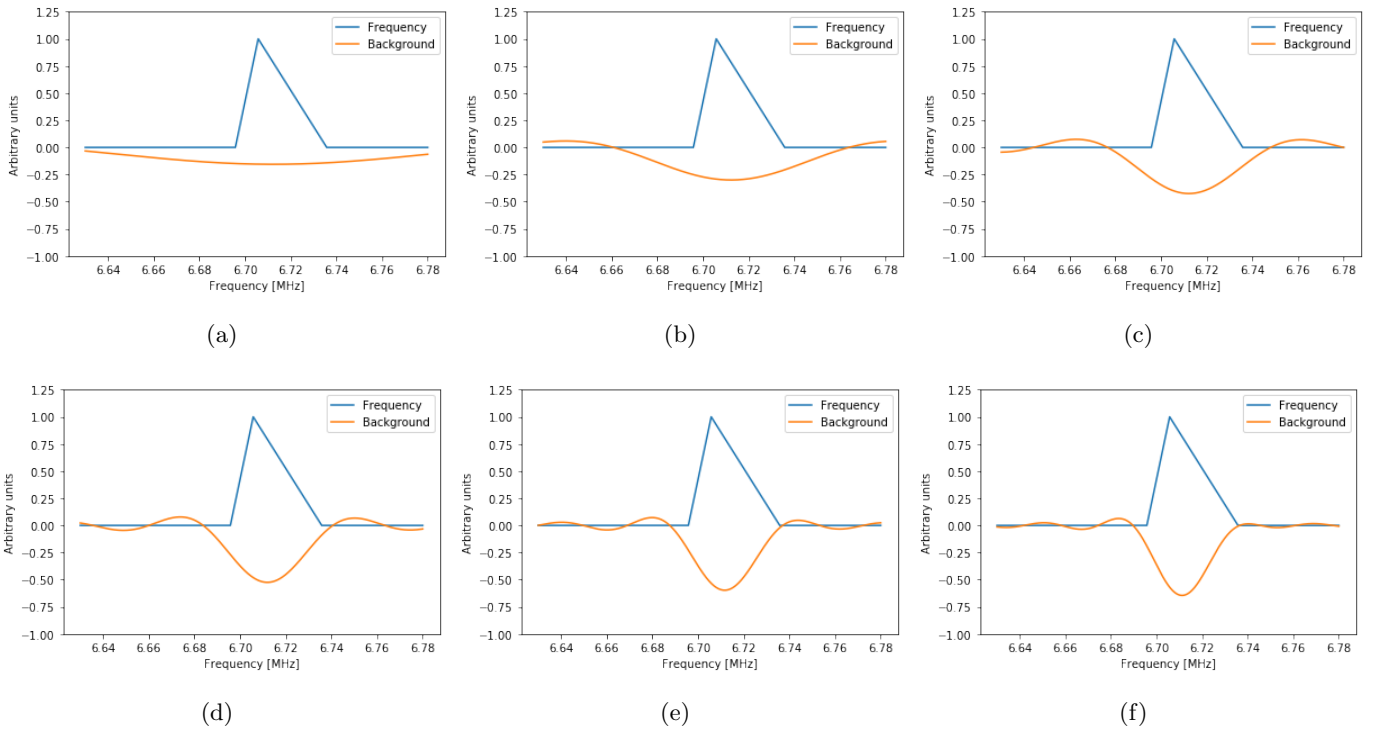


Figure 6: Background with  $t_0 = 0 \mu\text{s}$  and different values of  $t_s$  for a triangular frequency distribution centered at the magic frequency left bound of -10 kHz and right bound +30 kHz from its center. Six start times are shown: (a)  $5 \mu\text{s}$ , (b)  $10 \mu\text{s}$ , (c)  $15 \mu\text{s}$ , (d)  $20 \mu\text{s}$ , (e)  $25 \mu\text{s}$ , (f)  $30 \mu\text{s}$ .

## 169 2.5 Discussion of other possible analytic forms

170 We have been able to derive the analytic form of the correction to the cosine Fourier transformation using  
171 four different ansatzes for the frequency distribution. There are not many frequency distributions which can  
172 be plugged into (3) to get an analytic solution. In section 4 and 5 we show how the triangular frequency  
173 distribution can be fitted to both a Gaussian and asymmetric frequency distribution backgrounds so we have  
174 succeeded in our goals.

175 A possible improvement over the Gaussian frequency distribution for fitting asymmetric frequency distribu-  
176 tions would be to use a skewed-Gaussian frequency distribution defined by (37). Deriving a usable analytic form  
177 of the background for a skewed-Gaussian is very challenging since we would have to integrate it in equation(3).

178 An other improvement could be to use instead of a triangular frequency distribution, a higher order polygon.  
179 This complicates things however, since for each additional order of the polygon, we require an additional  
180 parameter to be fitted. The triangle frequency distribution is the most practical since it requires the least  
181 amount of parameters to fully describe the background.

## 182 3 Analytic background comparisons of the cosine Fourier transform

183 In this section we will compare how all of the analytic models for the background to the cosine Fourier transform  
184 are equivalent when  $t_s$  is small, but diverge for large values of  $t_s$ . In appendixes B and C we show how we  
185 can Taylor expand the different analytic forms to show how these various functions are equivalent in the limit  
186 where  $t_s$  is small and the frequency distribution is approximately symmetric.

### 187 3.1 Comparison of the delta, step, Gaussian, and triangular backgrounds

188 Figure 7 shows the comparison of the different analytic forms of the background to the cosine Fourier transfor-  
189 mation derived in section 2. We normalize the background for comparison purposes.

190 We can see that the backgrounds almost exactly overlay with each other. It is not until late start times where  
191 the backgrounds begin to show the forms of the frequency distributions which they came from. For  $t_s = 30 \mu s$ ,  
192 the delta function background is diverged from the step function, Gaussian, and triangular backgrounds. The  
193 step function, Gaussian, and triangular backgrounds behave similarly at  $30 \mu s$ , however the triangular function  
194 has the special feature that it can incorporate asymmetries in the frequency distribution which can not be seen  
195 in this figure since the background is symmetric.

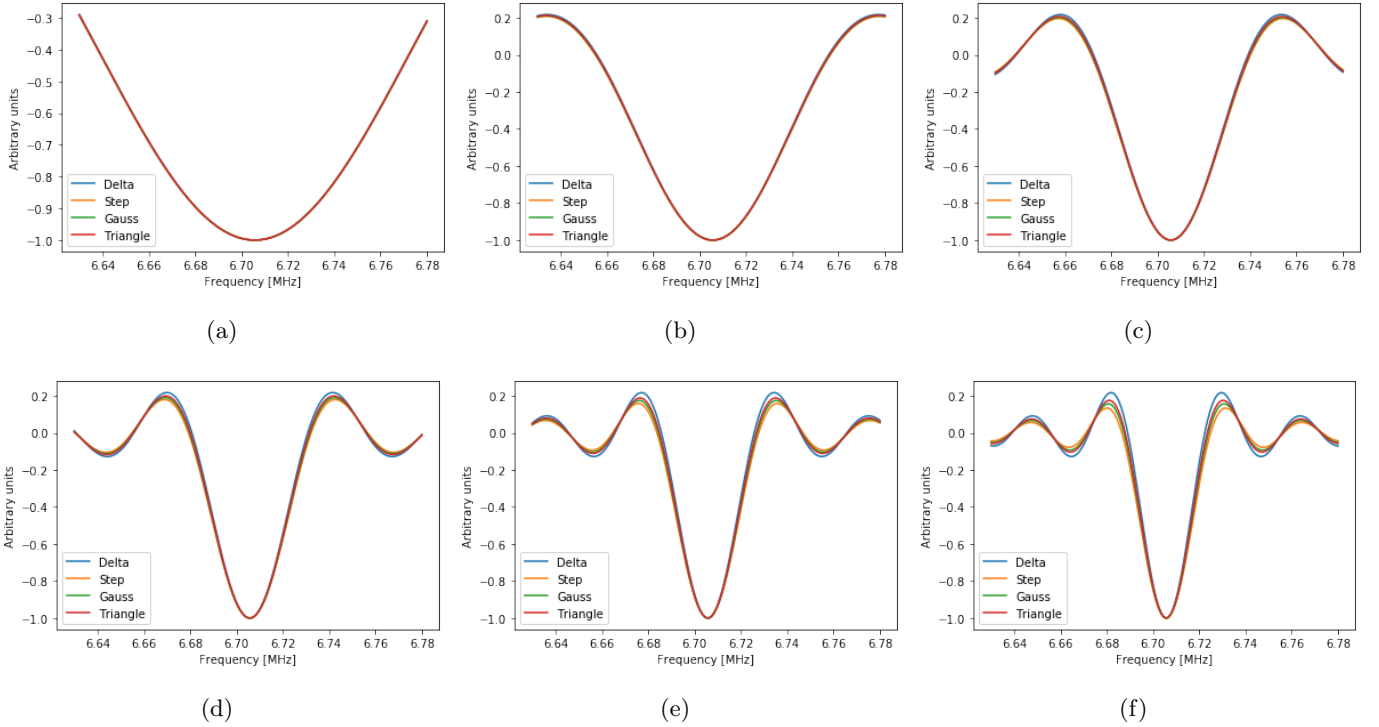


Figure 7: Background with  $t_0 = 0 \mu\text{s}$  and different values of  $t_s$  for the delta function, step function, Gaussian, and triangle backgrounds used in figures [2,3,4,5]. Six start times are shown: (a)  $5 \mu\text{s}$ , (b)  $10 \mu\text{s}$ , (c)  $15 \mu\text{s}$ , (d)  $20 \mu\text{s}$ , (e)  $25 \mu\text{s}$ , (f)  $30 \mu\text{s}$ .

### 196 3.2 The background cancels the frequency distribution at late start times

197 In figure 8 we show the background compared to the delta function, step function, Gaussian, and triangular  
 198 frequency distributions for a start time of  $200 \mu\text{s}$ . The amplitude of the distributions is arbitrary so we normalize  
 199 for the comparison. Note that we also do this for the delta function even though it is infinite.

200 We can see that using this very late start time, the background approximately matches the frequency  
 201 distribution. The cosine Fourier transformation is the frequency distribution plus the correction, so for large  
 202 start times the background completely cancels out the frequency distribution making it impossible to recover  
 203 the complete frequency distribution.

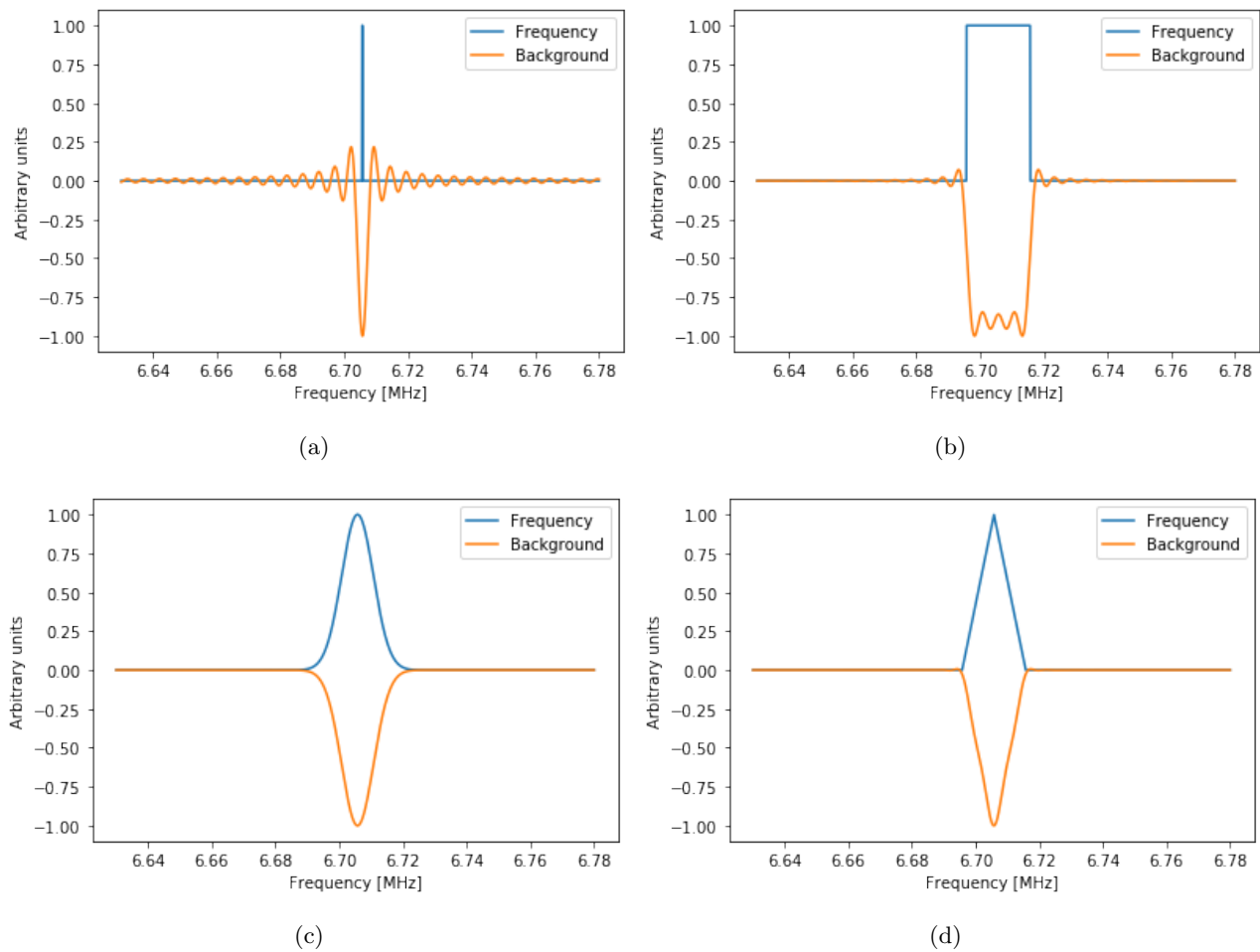


Figure 8: Background Comparison with  $t_0 = 0 \mu\text{s}$  and a large start time of  $t_s = 200 \mu\text{s}$  between Gaussian, step function, and triangular frequency distributions used in figures [2,3,4,5]. Four functions are shown: (a) Delta, (b) Step Function, (c) Gaussian, (d) triangle.

204 **4 Monte Carlo fitting with a Gaussian frequency distribution**

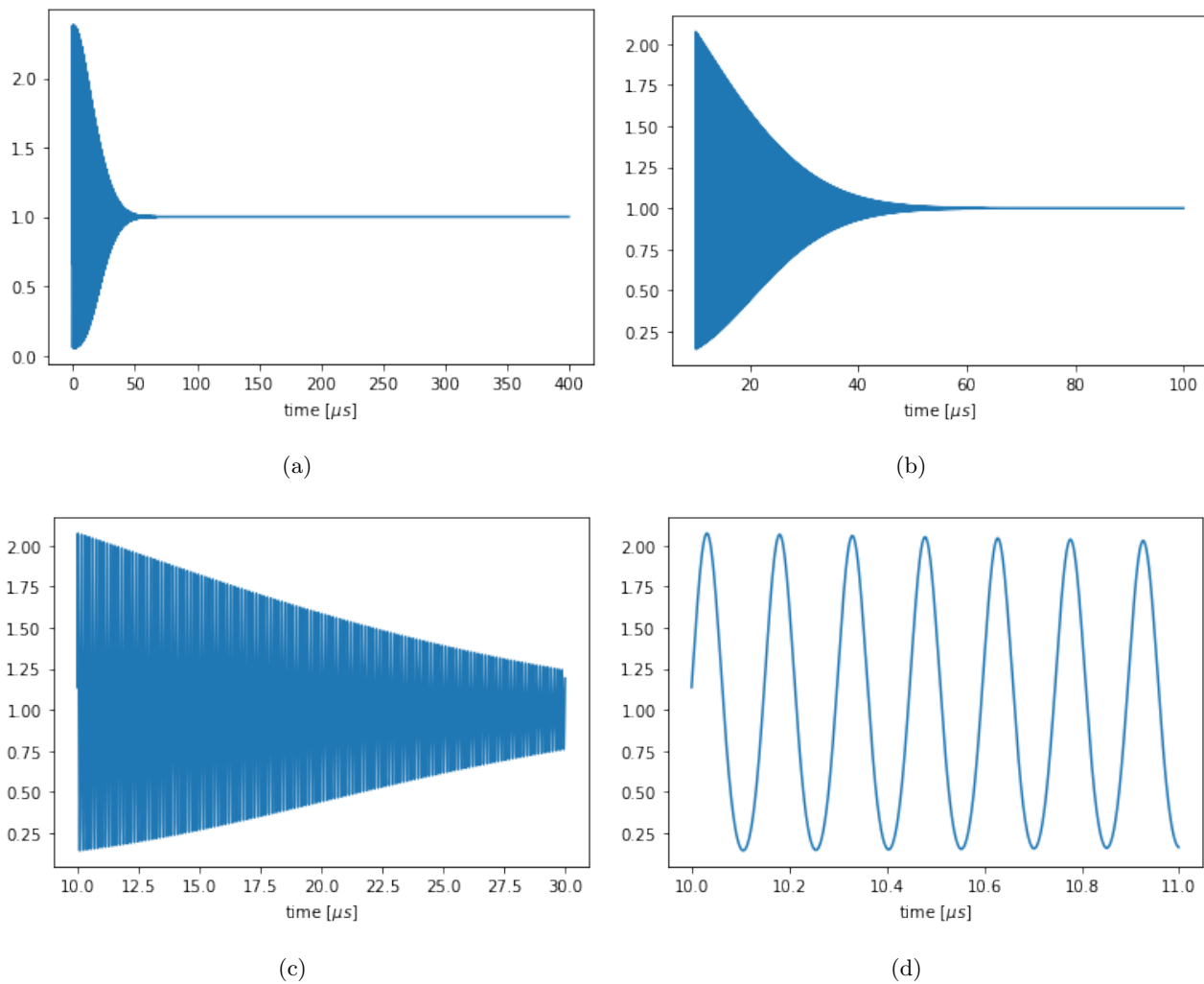


Figure 9: Fast rotation signal as a function of time generated by a Monte Carlo simulation [3]. The fast rotation signal has a Gaussian frequency distribution and longitudinal beam profile. The Frequency distribution is centered at the magic frequency with a fractional energy offset of 0.16% and the longitudinal beam profile is centered at  $0 \mu\text{s}$  with a standard deviation of 25 ns. Four time intervals are shown: (a)  $0\text{-}400 \mu\text{s}$ , (b)  $10\text{-}100 \mu\text{s}$ , (c)  $10\text{-}30 \mu\text{s}$ , (d)  $10\text{-}11 \mu\text{s}$ .

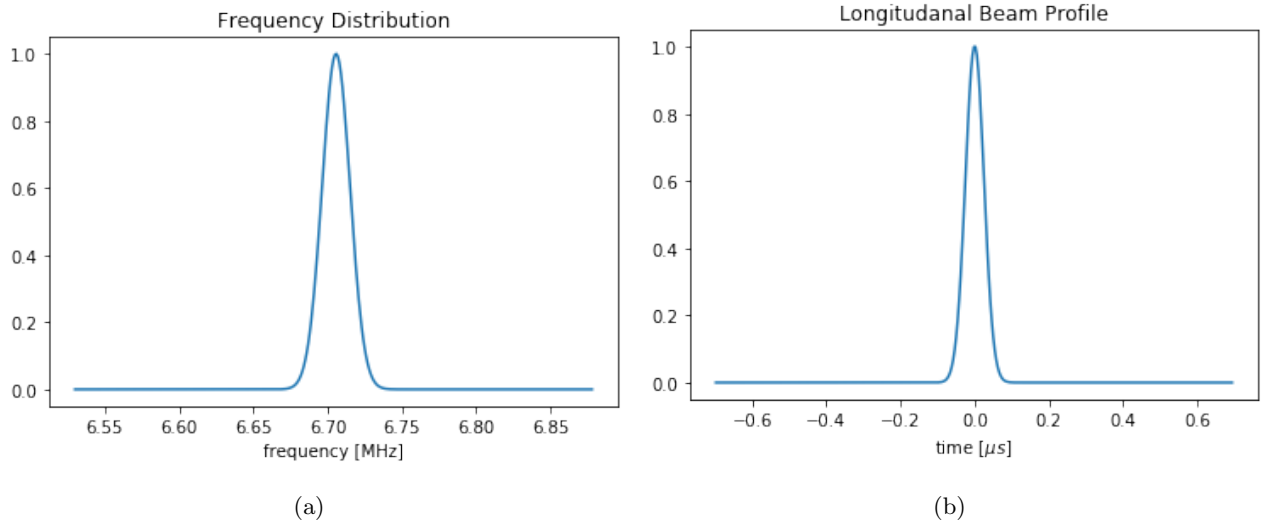


Figure 10: The Gaussian frequency distribution and longitudinal beam profile used in the Monte Carlo fast rotation signal shown in figure 9. (a) Frequency distribution, (b) Longitudinal beam profile.

205 In figures 9 and 10 we show a Monte Carlo fast rotation signal and the frequency distribution and longitudinal  
 206 beam profile used to make it. The Monte Carlo is created using the analytic form of the fast rotation signal  
 207 without noise nor statistical fluctuation [3]. We use this pristine fast rotation signal to test the background  
 208 fitting for the different functions.

209 In figure 11 we show the cosine Fourier transformation of the fast rotation signal for different values of  $t_s$ .  
 210 In appendix A we discuss how the width of the frequency distributions limits how large  $t_s$  can be and still have  
 211 the approximate forms for the background to the cosine Fourier transformation be valid. For this Monte Carlo  
 212 simulation, we use a frequency distribution wider than what is found in the data since we want to find the  
 213 upper limits of  $t_s$  that allows us to reliably recover the frequency distribution.

214 For large values of  $t_s$ , the background distorts the main peak of the cosine Fourier transformation and it will  
 215 no longer resemble the actual frequency distribution. This is because by  $t_s = 20 \mu s$  the width of the main peak  
 216 begins to get smaller as the background merges with it. For the small start time of  $t_s = 5 \mu s$  the background  
 217 on the cosine Fourier transformation is approximately parabolic and does not interfere with the actual signal.

218 The background is fitted to the cosine Fourier transformation using frequencies a distance away from the  
 219 minima which we specify in each figure. The fitted background is subtracted from the cosine Fourier trans-  
 220 formation to recover the original frequency distribution. This is the simplest way of recovering the frequency,  
 221 but we can use the full Fourier method for more accuracy [1]. The results of our analysis underperforms what  
 222 would be obtained using the full method.

223 **Important note:** In this note the E-field correction is calculated using the linear approximation [1]. For  
 224 Monte Carlo simulations the field index is arbitrary so we use a value of  $n = 0.1075$  which to match the Run-1  
 225 60-hour data set.

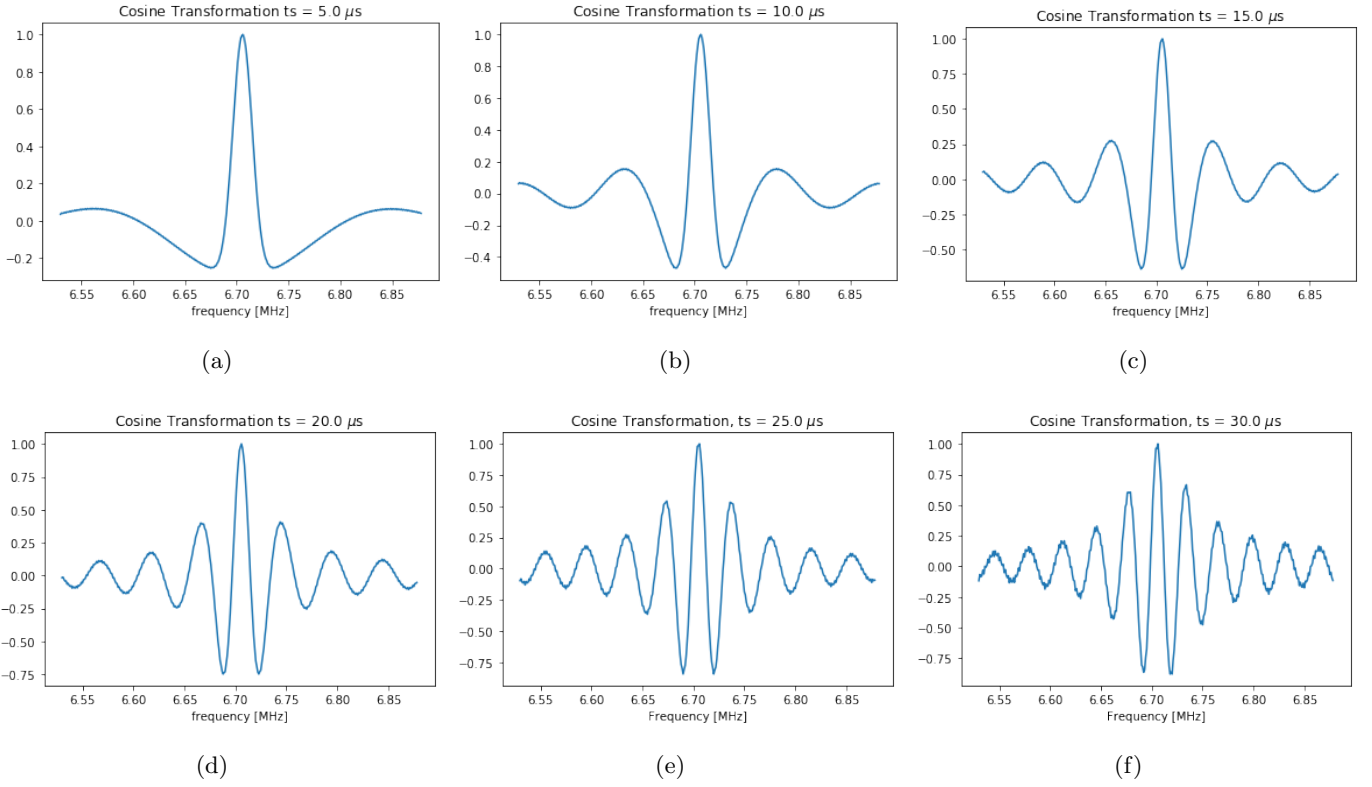


Figure 11: cosine Fourier transformation of the Monte Carlo in figure 9 using the correct value of  $t_0$  with different values of  $t_s$ . Six start times are shown: (a)  $5 \mu\text{s}$ , (b)  $10 \mu\text{s}$ , (c)  $15 \mu\text{s}$ , (d)  $20 \mu\text{s}$ , (e)  $25 \mu\text{s}$ , (f)  $30 \mu\text{s}$ .

## 226 4.1 polynomial

227 We can Taylor expand any of the analytic forms of the background which we derived, so we know that the  
 228 background can be fitted with a polynomial for small start times. In the following equation we show how we  
 229 can Taylor expand the sine function around  $\omega = \omega_0$  when  $|(\omega - \omega_0)(t_s - t_0)| \ll 1$ :

$$\begin{aligned}
 \Delta(\omega) &= \frac{1}{\pi} \frac{\sin[(\omega - \omega_0)(t_s - t_0)]}{(\omega - \omega_0)} \\
 &= \frac{1}{\pi} \frac{1}{(\omega - \omega_0)} \sum_{n=0}^{\infty} \frac{(-1)^n [(\omega - \omega_0)(t_s - t_0)]^{2n+1}}{(2n+1)!} = \frac{(t_s - t_0)}{\pi} \sum_{n=0}^{\infty} \frac{(-1)^n [(\omega - \omega_0)(t_s - t_0)]^{2n}}{(2n+1)!} \\
 &= \frac{(t_s - t_0)}{\pi} \left( 1 - \frac{[(\omega - \omega_0)(t_s - t_0)]^2}{3!} + \frac{[(\omega - \omega_0)(t_s - t_0)]^4}{5!} - \frac{[(\omega - \omega_0)(t_s - t_0)]^6}{7!} + \dots \right).
 \end{aligned} \tag{20}$$

230 This is the simplest way of fitting the background since it does not require any knowledge of the shape of  
 231 the background because each coefficient of the polynomial is fitted without having to give any initial values.

232 In appendix A we discuss how when  $t_s$  is small the background is approximately parabolic. For this small  
 233 start time, we only need a degree 2 polynomial to fit the background. If we use a higher order polynomial then  
 234 we can use some larger values of  $t_s$ .

235 We show in figure 12 that the background can be fitted with a degree 6 polynomial for  $t_s = 5 \mu\text{s}$ . There  
 236 does not seem to be any downside to using more orders of the polynomial, so we use 6 terms of the polynomial

237 which is more than enough.

238 Figure 13 shows that by  $10 \mu\text{s}$ , the background is too highly-nonlinear and not of polynomial form to be  
 239 fitted. To skip scraping we will have to use more sophisticated fit functions, however the polynomial fit is more  
 240 than sufficient to skip the beam-line positron contamination of the muon beam

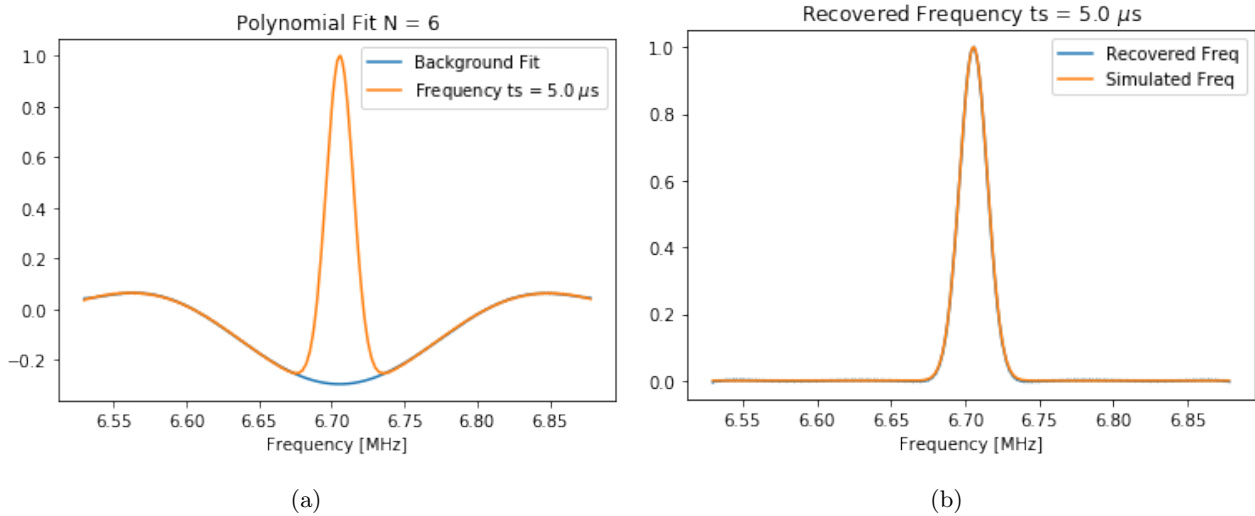


Figure 12: Fitting the background with a polynomial fit of degree 6 with  $t_s = 5 \mu\text{s}$  fitting 0.5 kHz away from minima. (a) Fitted cosine Fourier transformation (b) Recovered Frequency Distribution.

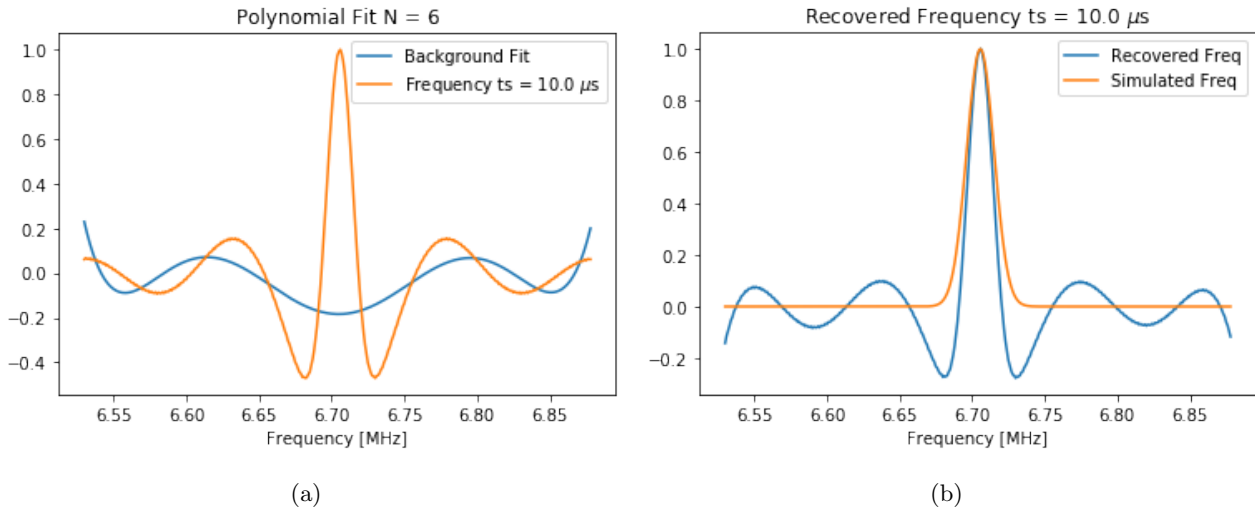


Figure 13: Fitting the background with a polynomial fit of degree 6 with  $t_s = 10 \mu\text{s}$  fitting 0.5 kHz away from minima. (a) Fitted cosine Fourier transformation,  $C_E = -378.04 \text{ ppb}$  (b) Recovered Frequency Distribution,  $C_E = -359.52 \text{ ppb}$ .

## 241 4.2 sinc

242 We showed in section 2.1 that we can approximate the frequency background using a sinc function in equation  
 243 (6). This enables us to fit the background outside the signal with a sinc function. The amplitude of the  
 244 background is arbitrary so we fit the background as the following:

$$\Delta(\omega) = -A \operatorname{sinc}[(\omega - \omega_0)t], \quad (21)$$

245 where the parameters  $A$ ,  $\omega_0$ , and  $t$  are fitted to match the distribution. The parameter  $t$  represents  $t_s - t_0$ .  
 246 We could include an additive constant term to the background fit as well, but it does not make any difference  
 247 on the fit as it will be fitted to nearly zero. We therefore do not included an additive constant for any of our  
 248 fit functions.

249 Figure 14 shows the sinc background fit for  $t_s = 5 \mu\text{s}$ . This fits the background well with a  $C_E$  difference  
 250 of only 13.42 ppb. For large values of  $t_s$ , the background cannot be fitted as well. We show in figure 15 that  
 251 the sinc function being fitted to the background for  $t_s = 30 \mu\text{s}$  which yields a large  $C_E$  difference of 222.2 ppb.  
 252 The sinc function will outperform the polynomial fit, however still falters for values of  $t_s$  greater than  $15 \mu\text{s}$ .

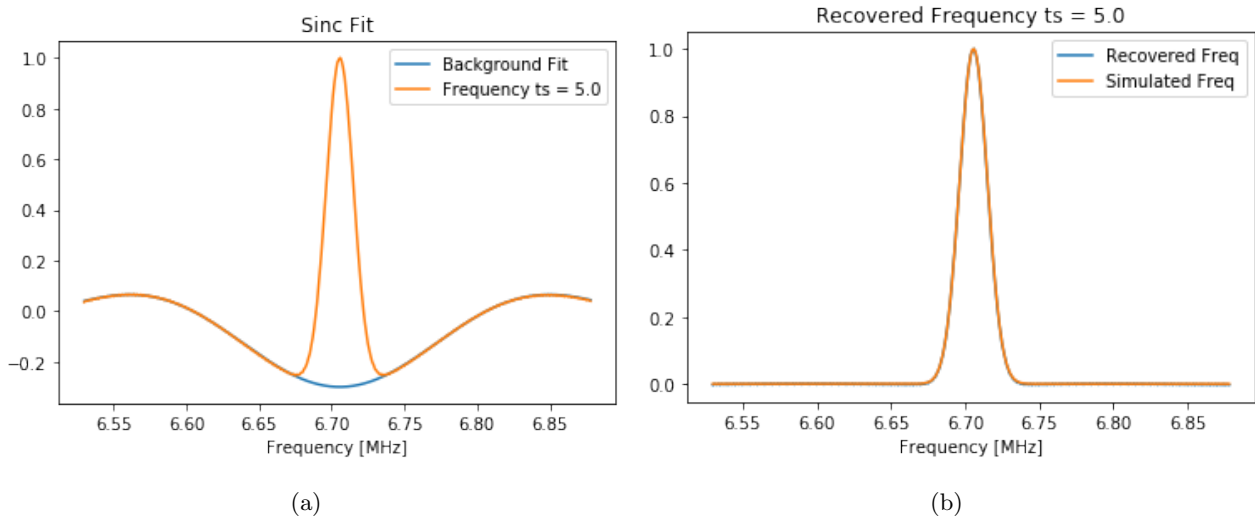


Figure 14: Fitting the background with a sinc function with  $t_s = 5 \mu\text{s}$  fitting 2.0 kHz away from the minima. (a) Fitted cosine Fourier transformation,  $C_E = -378.04$  ppb (b) Recovered Frequency Distribution,  $C_E = -379.70$  ppb.

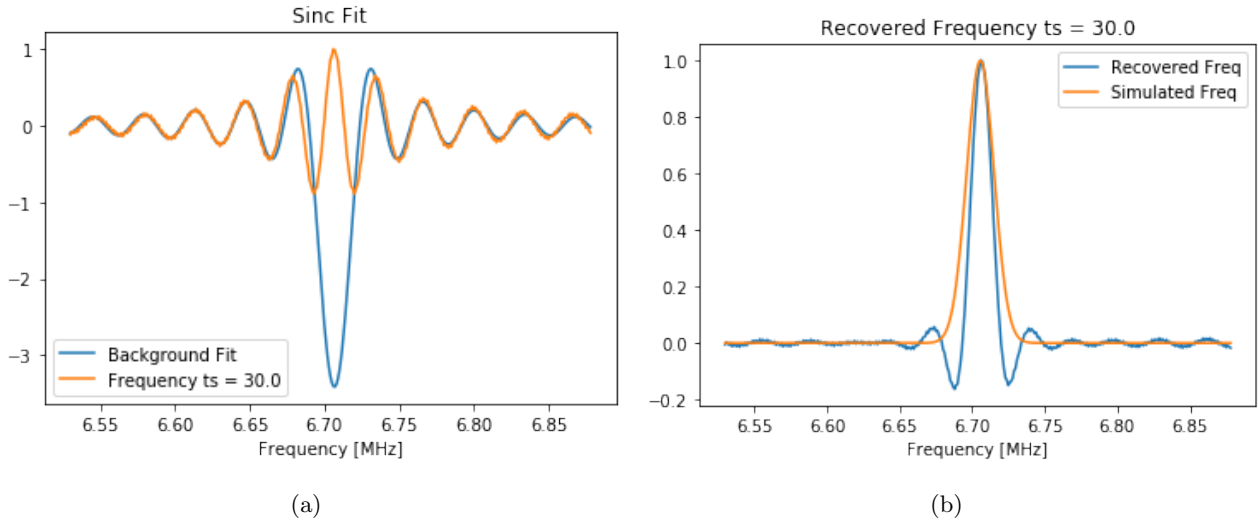


Figure 15: Fitting the background with a sinc function with  $t_s = 30 \mu\text{s}$  fitting 2.0 kHz away from the minima. (a) Fitted cosine Fourier transformation,  $C_E = -378.04$  ppb (b) Recovered Frequency Distribution,  $C_E = -167.82$  ppb.

### 253 4.3 Si

254 We showed in section 2.2 to be Si functions of the form in equation (22). With an arbitrary amplitude we  
 255 approximate the form of the background to be:

$$\Delta(\omega) = -A[\text{Si}((\omega - \omega_1)t) - \text{Si}((\omega - \omega_2)t)], \quad (22)$$

256 where the fit parameters  $A$ ,  $\omega_1$ ,  $\omega_2$ , and  $t$ . We see in figure 16 that for  $t_s = 5 \mu\text{s}$  the background is fitted  
 257 very well with a difference in  $C_E$  of only 1.66 ppb. For  $t_s = 15 \mu\text{s}$  as shown in figure 17, we are still able to  
 258 fit the background using with this analytic form yielding only a small  $C_E$  difference of 8.35 ppb. For  $t_s = 30$   
 259  $\mu\text{s}$ , the Si function fits the background decently, but there is still a large  $C_E$  difference of 154.0 ppb since the  
 260 frequency distribution includes negative values.

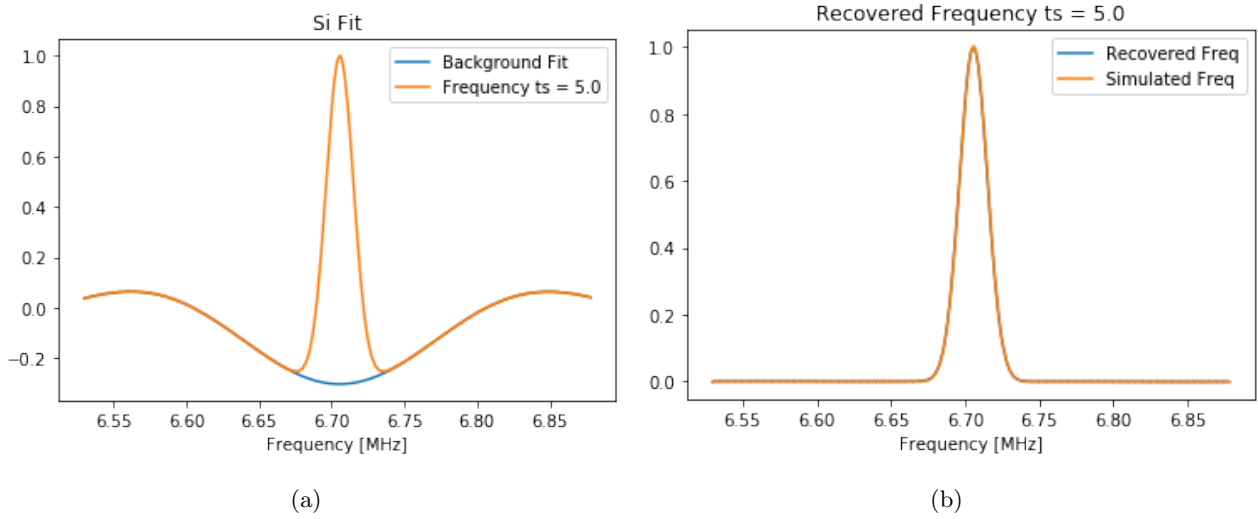


Figure 16: Fitting the background with Si functions with  $t_s = 5 \mu s$  fitting 2.0 kHz away from the minima. (a) Fitted cosine Fourier transformation,  $C_E = -378.04$  ppb (b) Recovered Frequency Distribution,  $C_E = -379.70$  ppb.

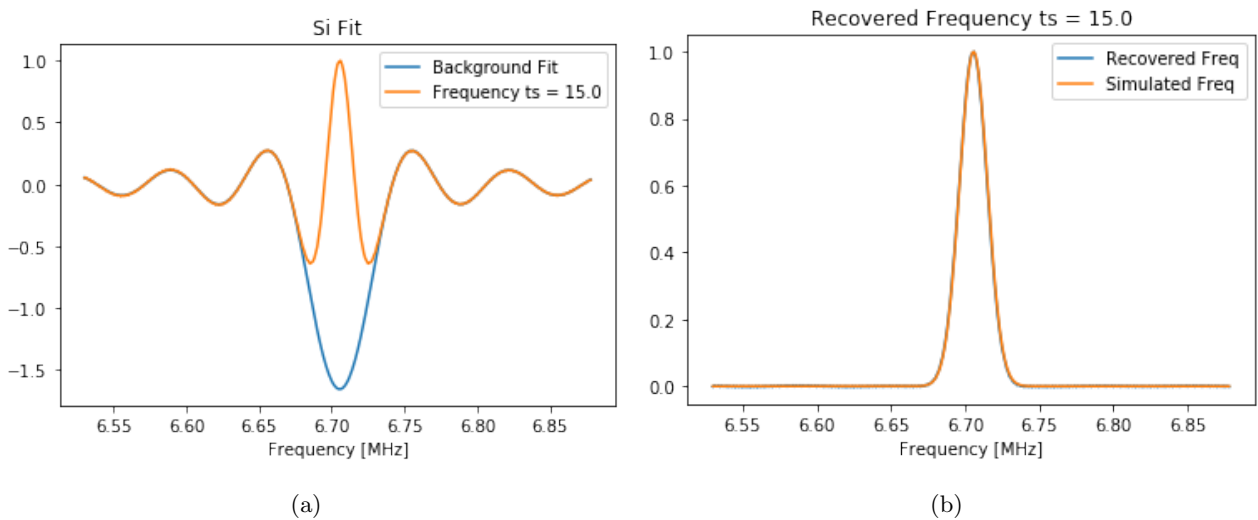


Figure 17: Fitting the background with Si functions with  $t_s = 15 \mu s$  fitting 2.0 kHz away from the minima. (a) Fitted cosine Fourier transformation,  $C_E = -378.04$  ppb (b) Recovered Frequency Distribution,  $C_E = -369.68$  ppb.

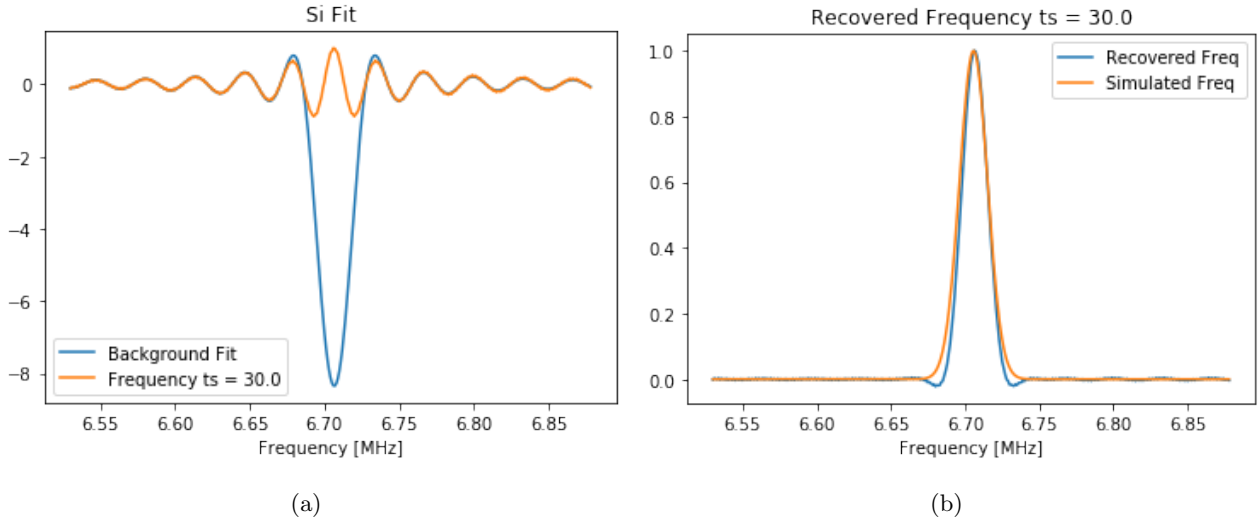


Figure 18: Fitting the background with a Si functions with  $t_s = 30 \mu s$  fitting 2.0 kHz away from the minima. (a) Fitted cosine Fourier transformation,  $C_E = -378.04$  ppb (b) Recovered Frequency Distribution,  $C_E = -224.03$  ppb.

#### 261 4.4 erfi

262 We derive in section 2.3 that the background for a Gaussian frequency distribution takes the form of equation  
 263 (16). With an arbitrary amplitude we use the fit function of the following form:

$$\Delta(\omega) = -Ae^{-\frac{(\omega-\omega_0)^2}{2\sigma^2}} \text{Im} \left\{ \text{erfi} \left( \frac{\omega - \omega_0 + i\sigma^2 t}{\sqrt{2}\sigma} \right) \right\}, \quad (23)$$

264 and we fit for the parameters  $A$ ,  $\sigma$ ,  $\omega_0$ , and  $t$ . Figure 19 shows that the background can be fitted well using  
 265 the erfi function for  $t_s = 5 \mu s$  yielding a  $C_E$  difference of only 1.66 ppb from the known answer. Unlike the  
 266 other background forms, we shown in figure 20 that we can fit the background using the erfi function for values  
 267 all the way up to  $t_s = 30 \mu s$  without problems. The difference in E-field correction at  $t_s = 30 \mu s$  is only 7.35  
 268 ppb, so we succeeded in our goal to use a value of  $t_s$  large enough to skip scraping for this Gaussian Monte  
 269 Carlo.

270 We should not be too surprised that we were able to fit the background all the way up to  $t_s = 30 \mu s$  since  
 271 we are using the exact analytic form of the background for a Gaussian frequency distribution, so we are not  
 272 making any approximations in the form of the background.

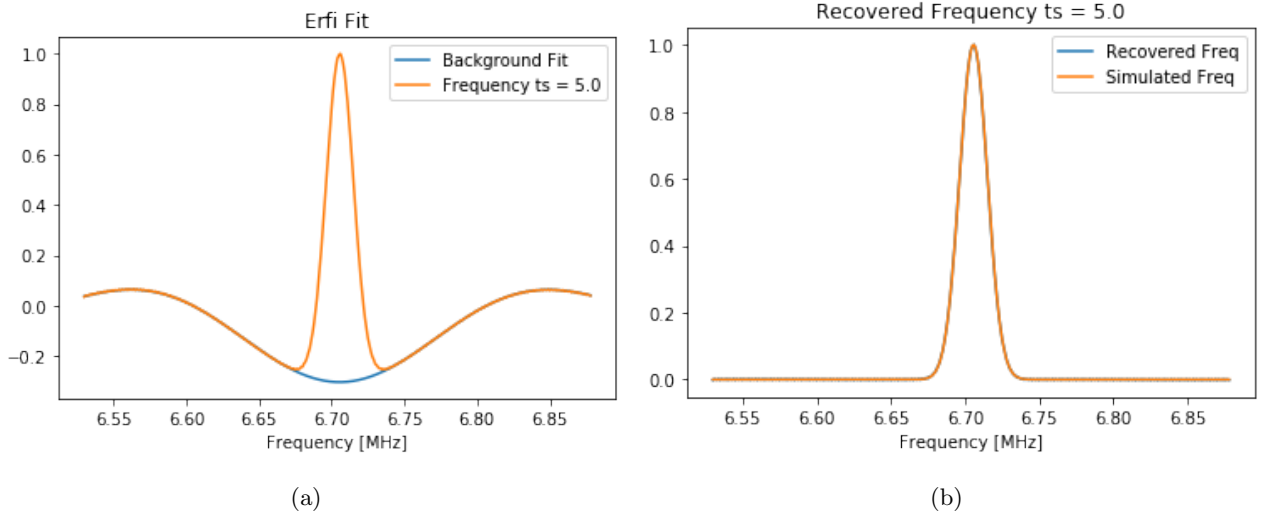


Figure 19: Fitting the background with a erfi function with  $t_s = 5 \mu s$  fitting 2.5 kHz away from the minima. (a) Fitted cosine Fourier transformation,  $C_E = -378.04$  ppb (b) Recovered Frequency Distribution,  $C_E = -379.70$  ppb.

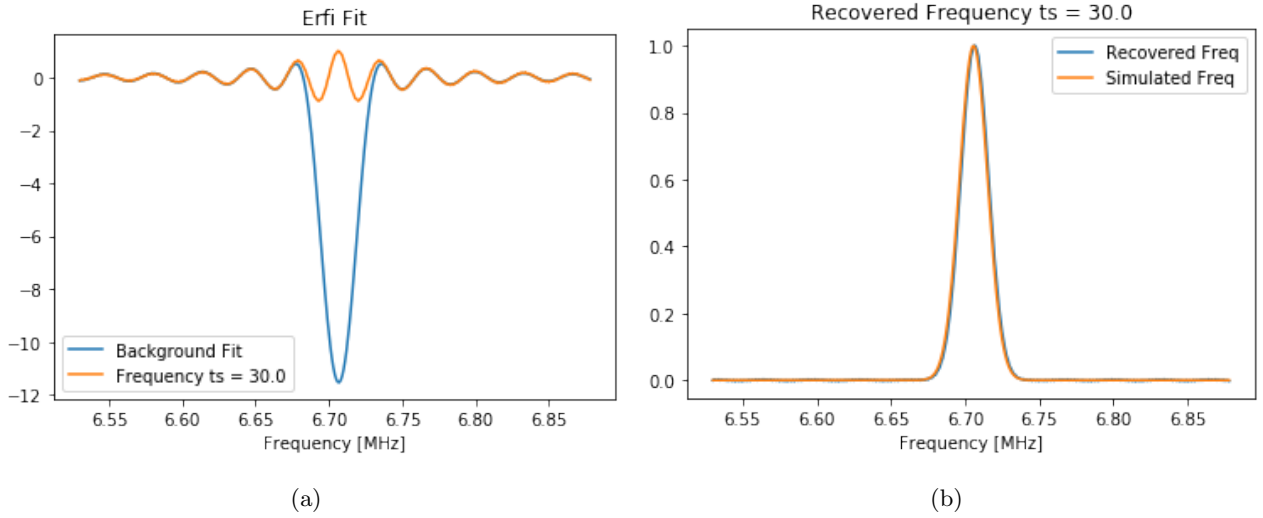


Figure 20: Fitting the background with a erfi function of degree 6 with  $t_s = 30 \mu s$  fitting 2.5 kHz away from the minima. (a) Fitted cosine Fourier transformation,  $C_E = -378.04$  ppb (b) Recovered Frequency Distribution,  $C_E = -385.39$  ppb.

## 273 4.5 Triangular

274 In section 2.4 we showed that a triangular frequency distribution produces a frequency background of the form  
 275 in equation (19). When we include an arbitrary amplitude we obtain the following form of the background:

$$\Delta(\omega) = -A \left[ \frac{\omega - \omega_1}{\omega_0 - \omega_1} [\text{Si}((\omega - \omega_1)t) - \text{Si}((\omega - \omega_0)t)] + \frac{\cos((\omega - \omega_1)t) - \cos((\omega - \omega_0)t)}{(\omega_0 - \omega_1)t} \right. \\ \left. + \frac{\omega_2 - \omega}{\omega_0 - \omega_2} [\text{Si}((\omega - \omega_1)t) - \text{Si}((\omega - \omega_0)t)] - \frac{\cos((\omega - \omega_2)t) - \cos((\omega - \omega_0)t)}{(\omega_0 - \omega_2)t} \right], \quad (24)$$

276 where the parameters  $A$ ,  $\omega_1$ ,  $\omega_2$ ,  $\omega_0$ , and  $t$  are fitted to the background. In figure 21 we show that for  
 277  $t_s = 5 \mu\text{s}$ , the background is fitted well with a  $C_E$  difference of only 0.321 ppb. For  $t_s = 15 \mu\text{s}$  as shown in  
 278 figure 22, the background can still be fitted using the triangle function with a  $C_E$  difference of 17.77 ppb.  
 279 When we use a very late start time like  $t_s = 30 \mu\text{s}$  shown in figure 23, the triangle function fits the background  
 280 decently, however we still get a large  $C_E$  difference of 97.22 ppb. This is similar to what happened when we  
 281 used the Si function.

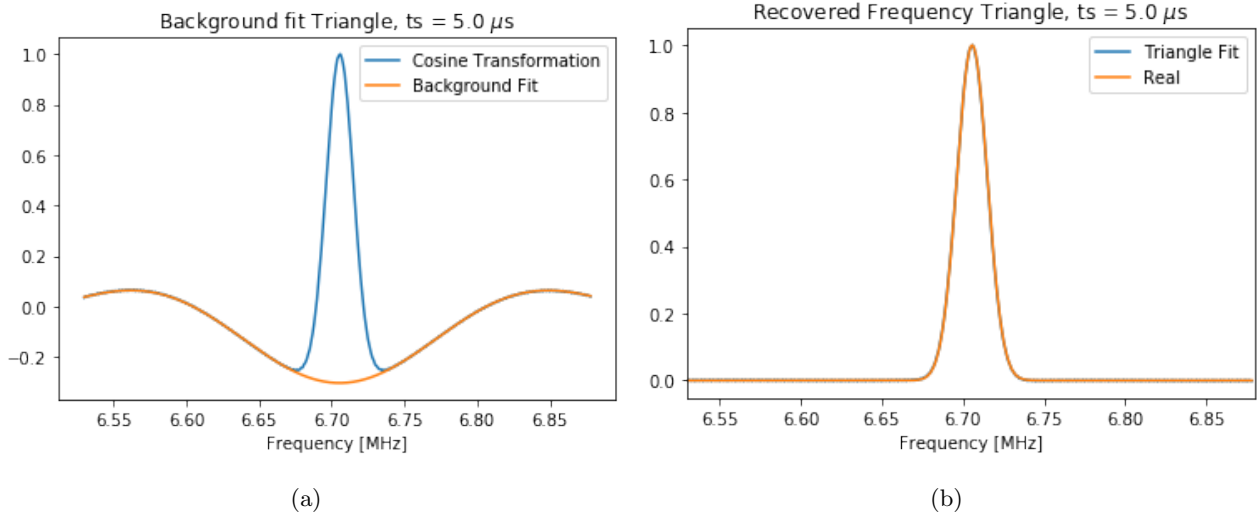


Figure 21: Fitting the background with the triangular background with  $t_s = 5 \mu\text{s}$  fitting 2.0 kHz away from the minima. (a) Fitted cosine Fourier transformation,  $C_E = -378.04$  ppb (b) Recovered Frequency Distribution,  $C_E = -378.35$  ppb.

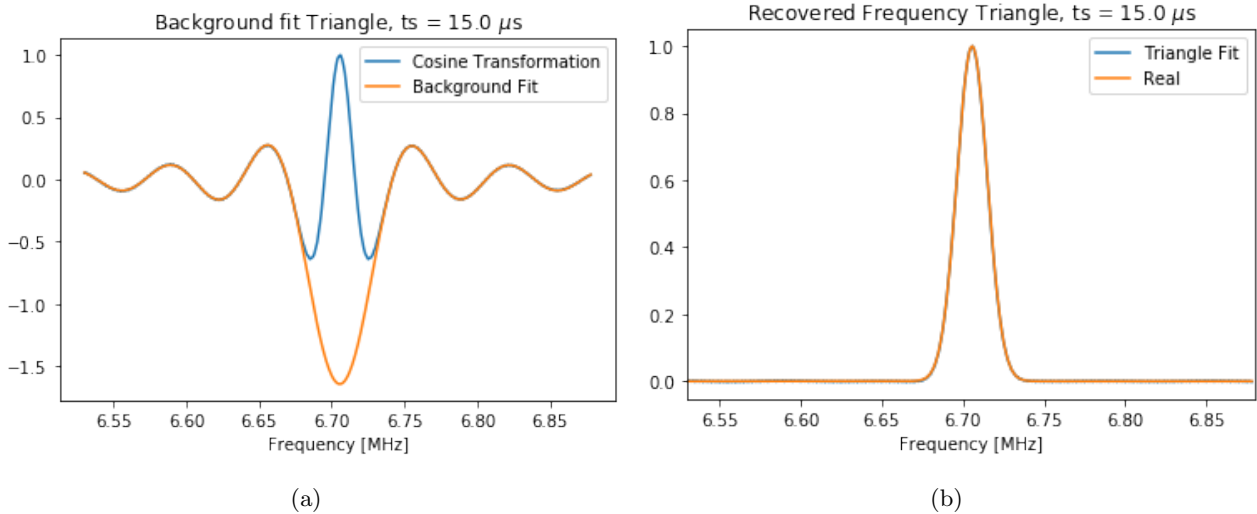


Figure 22: Fitting the background with the triangular background with  $t_s = 15 \mu\text{s}$  fitting 2.0 kHz away from the minima. (a) Fitted cosine Fourier transformation,  $C_E = -378.04$  ppb (b) Recovered Frequency Distribution,  $C_E = -360.27$  ppb.

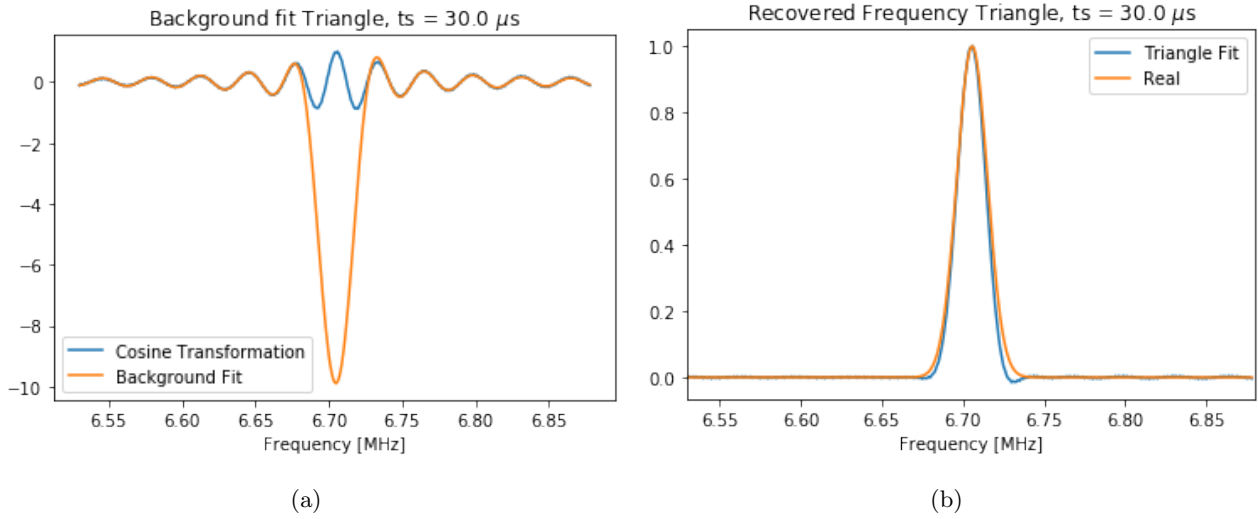


Figure 23: Fitting the background with the triangular background with  $t_s = 30 \mu s$  fitting 2.0 kHz away from the minima. (a) Fitted cosine Fourier transformation,  $C_E = -378.04$  ppb (b) Recovered Frequency Distribution,  $C_E = -280.82$  ppb.

## 282 5 Monte Carlo fitting with an asymmetric frequency distribution

283 We also want to test if the frequency background can be fitted using an asymmetric frequency distribution. In  
 284 figure 24 we show how the recovered frequency distribution for the Run-1 60-hour data set is asymmetric. We  
 285 will use the asymmetric frequency distribution shown in figure 24 which is used to generate the fast rotation  
 286 signal with a realistic longitudinal beam profile shown in figure 25.

287 This Monte Carlo also has statistical uncertainty with it which makes the cosine Fourier transformation  
 288 have a lot of statistical fluctuations when  $t_s$  is large. This is because the muon beam is completely debunched  
 289 around the ring by  $100 \mu s$  of the fast rotation signal, so skipping a large part of the fast rotation signal where  
 290 the muon beam has not yet debunched severely limits the statistics of the cosine Fourier transform. This can  
 291 be seen in figure 26 since when  $t_s$  is  $15 \mu s$  or less the cosine Fourier transformation is smooth, but for larger  
 292 values of  $t_s$  there are large statistical fluctuations.

293 We are now using an asymmetric frequency distribution, so we do not optimize for  $t_0$  for each values of  $t_s$ .  
 294 We instead find  $t_0$  once for  $t_s = 4 \mu s$  and then fix the value.

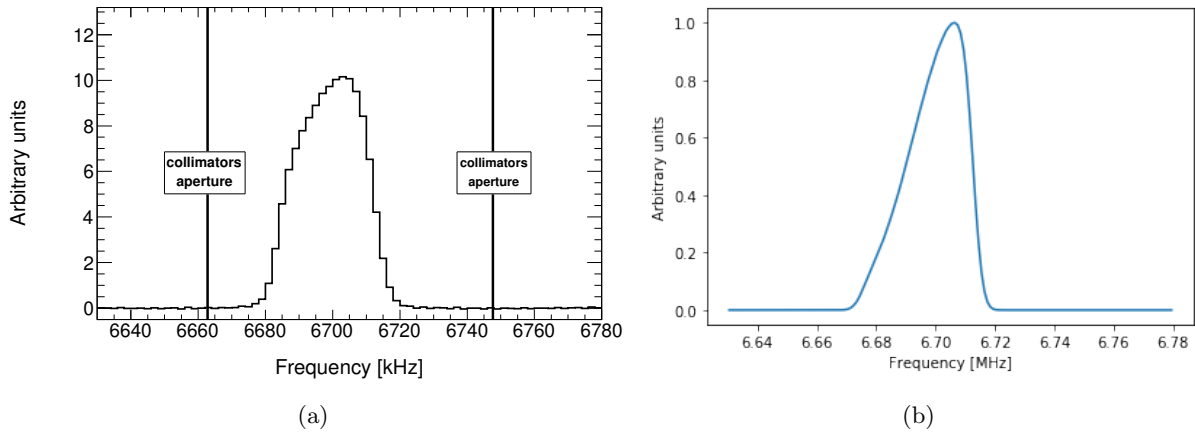


Figure 24: (a) This is the recovered frequency distribution of the Run-1 60-hour data set (b) a similarly asymmetric frequency distribution to be used in a Monte Carlo simulation.

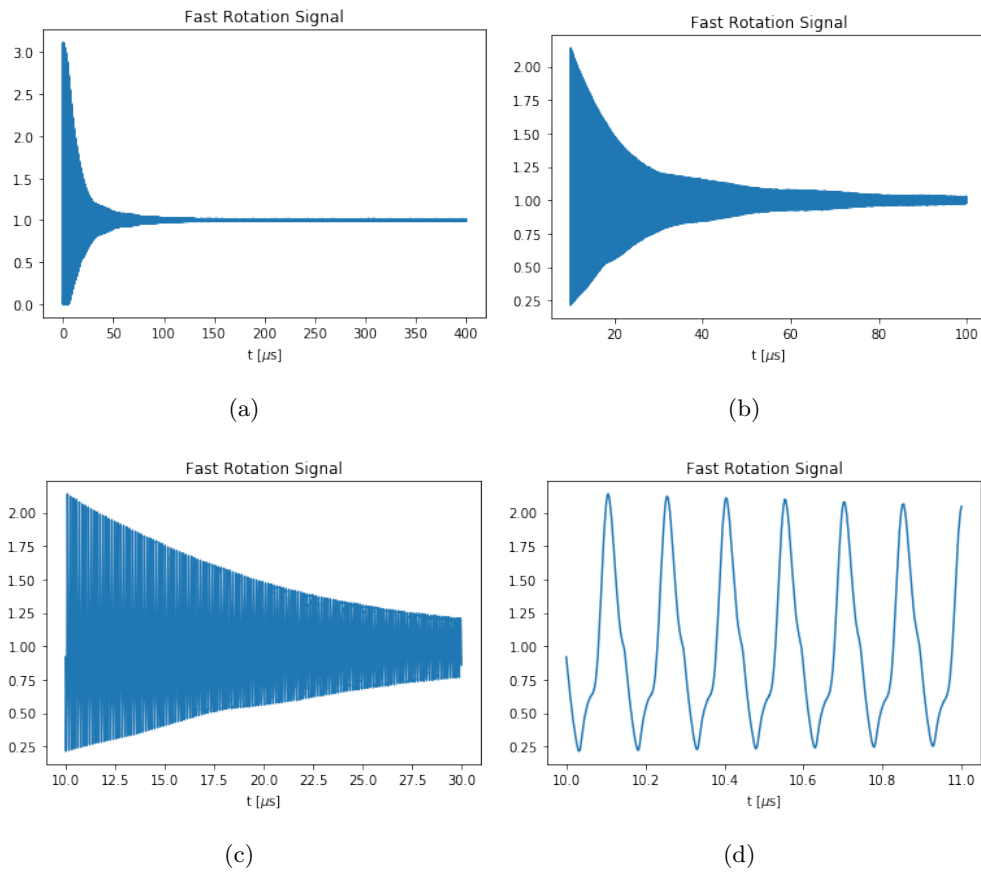


Figure 25: A fast rotation signal generated using a Monte Carlo simulation [4]. Four time intervals are shown: (a) 0-400  $\mu s$ , (b) 10-100  $\mu s$ , (c) 10-30  $\mu s$ , (d) 10-11  $\mu s$ .

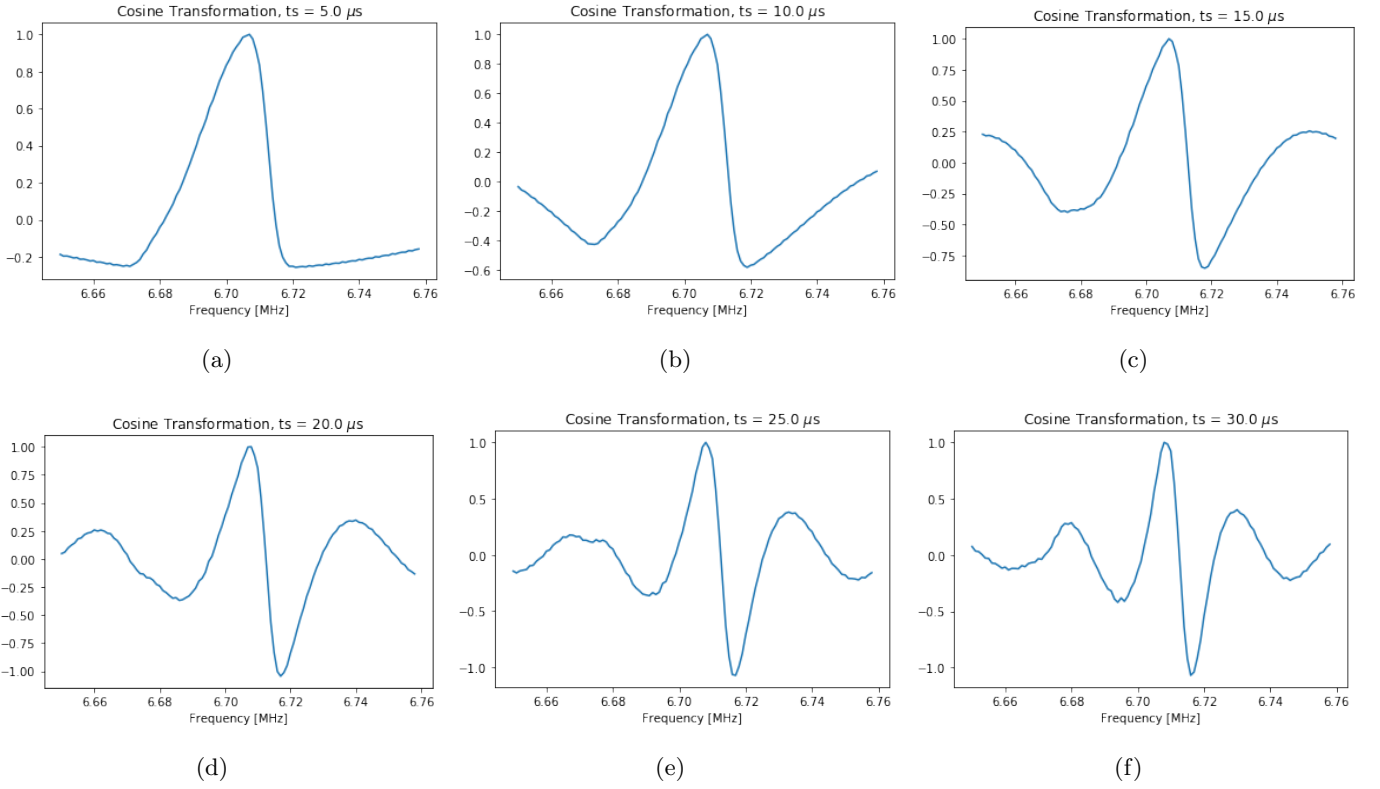


Figure 26: cosine Fourier transformation of the Monte Carlo simulation from figure 25 using a fixed value of  $t_0$  and different values of  $t_s$ . Six start times are shown: (a)  $5 \mu s$ , (b)  $10 \mu s$ , (c)  $15 \mu s$ , (d)  $20 \mu s$ , (e)  $25 \mu s$ , (f)  $30 \mu s$ .

## 295 5.1 Fit comparison

296 We show in figure 27 how the background can be fitted for using any of the fit functions for  $t_s = 5 \mu s$ . When we  
 297 use a larger start time like  $t_s = 15 \mu s$  shown in figure 28, the polynomial can no longer fit the background since  
 298 it is highly non-linear and no longer takes a polynomial form. The sinc function is also ineffective at fitting the  
 299 background because approximating the frequency distribution to be a delta function is no longer valid. For  $t_s =$   
 300  $25 \mu s$  shown in figure 29, the erfi and the Si functions can no longer be fitted to the background either since the  
 301 approximation that the background is a Gaussian or a step function is no longer valid since neither a Gaussian  
 302 or a step function can account for asymmetries. We see in figure 30 that the triangular background fit, on the  
 303 other hand, can fitted to the background all the way up to  $t_s = 30 \mu s$  since the triangular background can  
 304 account for asymmetries in the frequency distribution. For  $t_s = 30 \mu s$ , however, large statistical fluctuations  
 305 limit the ability to reasonably recover the complete frequency distribution. While the background can be fitted  
 306 decently, we show in the next section how the recovered E-field cannot be properly recovered.

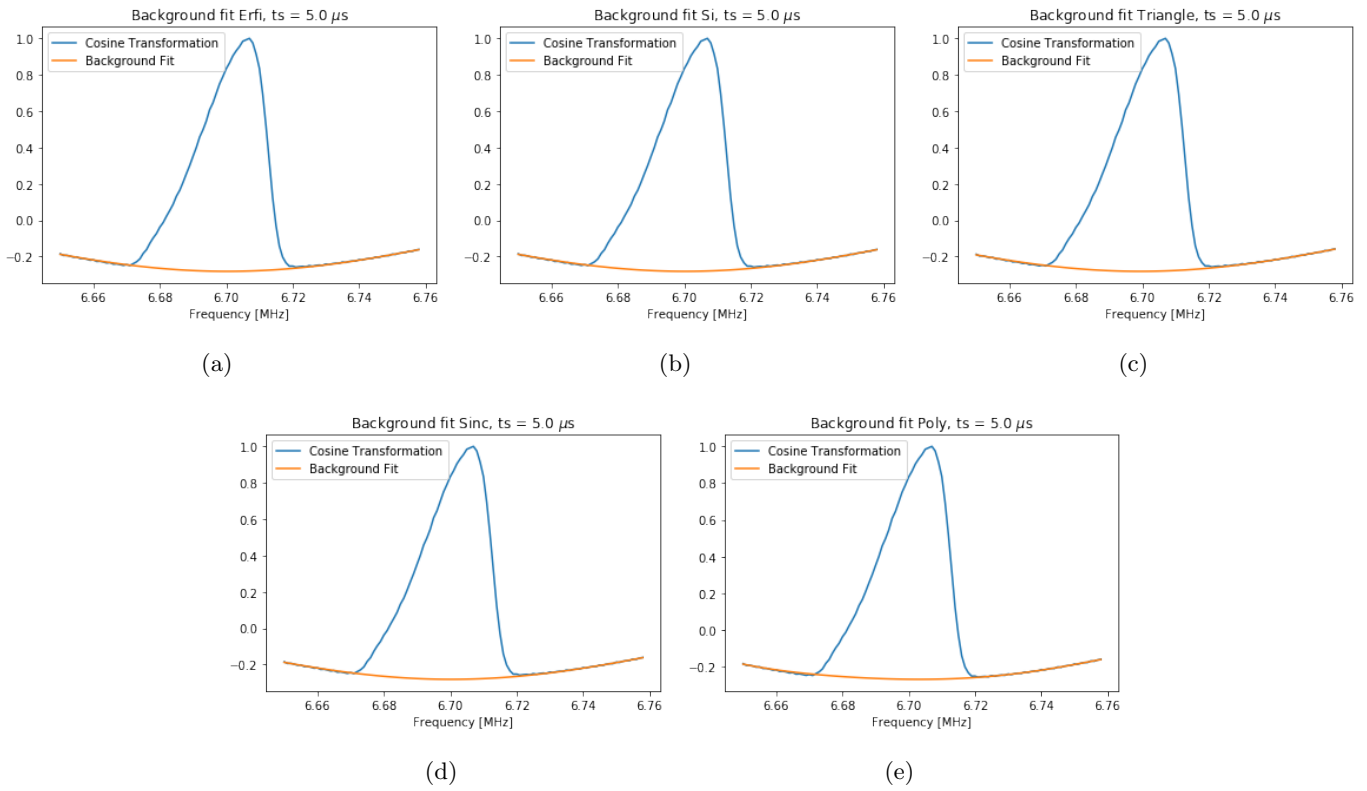


Figure 27: Fitting the frequency background 1.5 kHz away from the minima with  $t_s = 5 \mu s$ . The five fit functions are shown: (a) erfi, (b) Si, (c) triangle, (d) sinc, (e) poly.

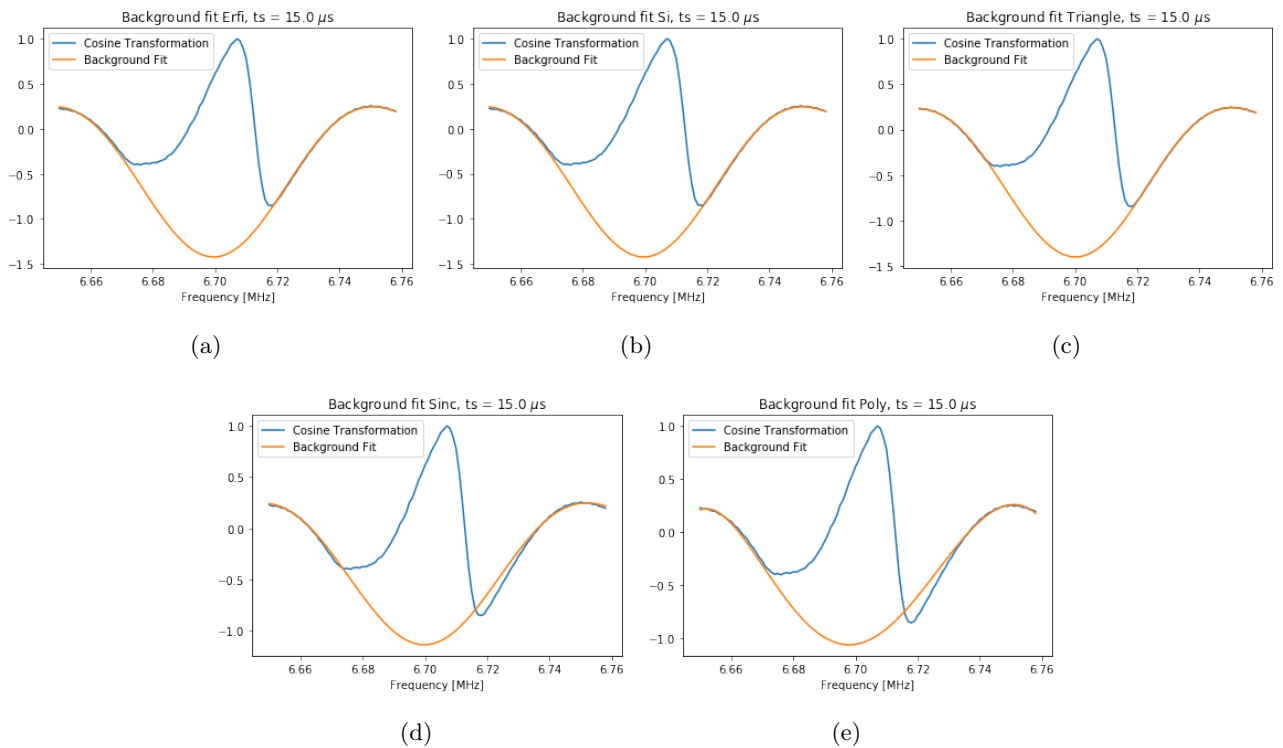


Figure 28: Fitting the frequency background 1.5 kHz away from the minima with  $t_s = 15 \mu s$ . The five fit functions are shown: (a) erfi, (b) Si, (c) triangle, (d) sinc, (e) poly

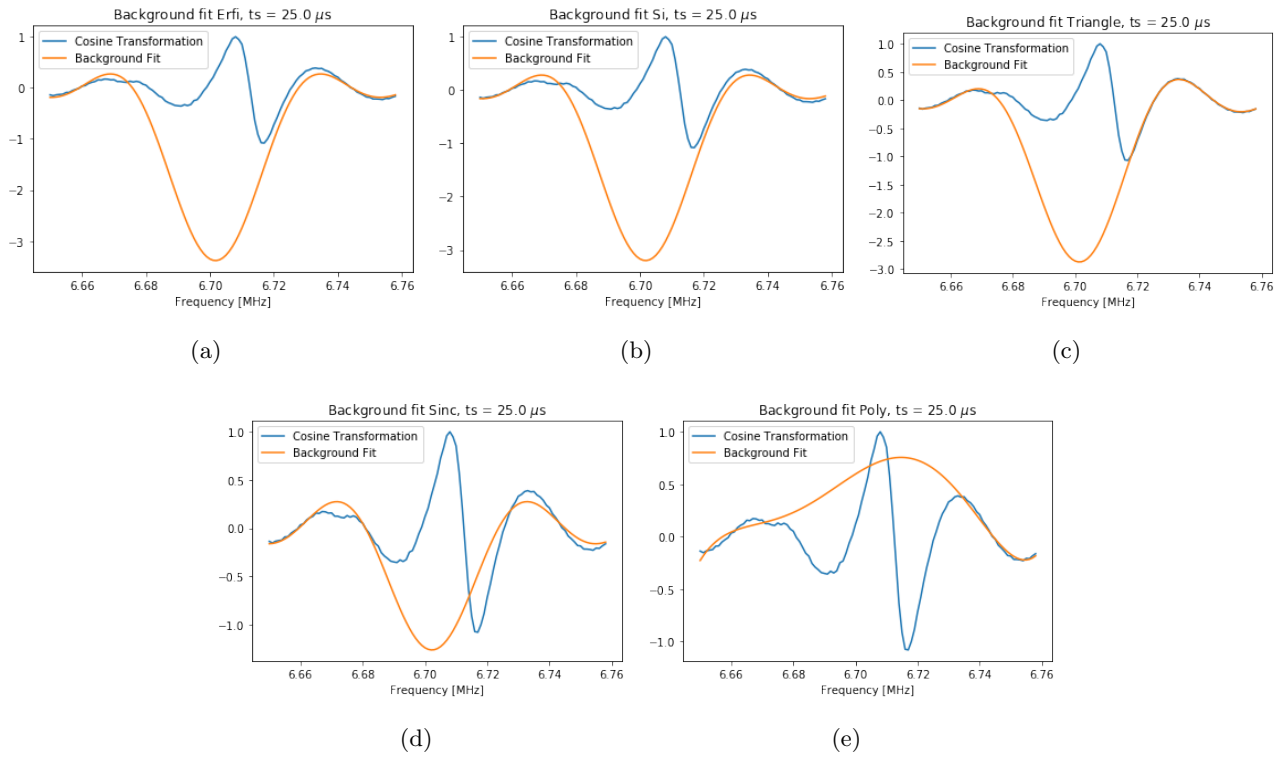


Figure 29: Fitting the frequency background 1.5 kHz away from the minima with  $t_s = 25 \mu s$ . The five fit functions are shown: (a) erfi, (b) Si, (c) triangle, (d) sinc, (e) poly.

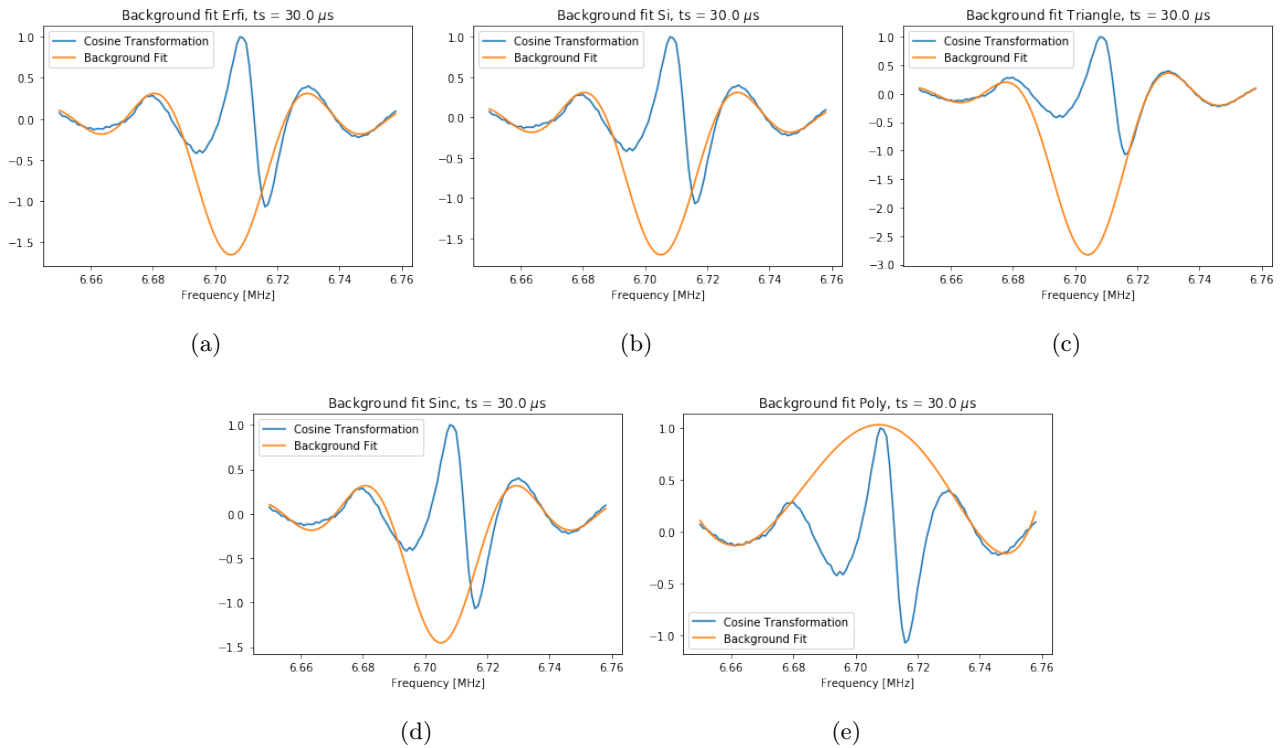


Figure 30: Fitting the frequency background 1.5 kHz away from the minima with  $t_s = 30 \mu s$ . The five fit functions are shown: (a) erfi, (b) Si, (c) triangle, (d) sinc, (e) poly.

307 **5.2 E-field comparison**

308 We showed in the previous section how the background can be fitted for different start times. In figure 31 we  
 309 show how the difference in the recovered E-field and the actual E-field corrections change with increasing values  
 310 of  $t_s$ .

311 The polynomial fit can recover the E-field correction up to about  $10 \mu s$  before it can no longer be fitted to  
 312 the background. The sinc fit is valid for about  $13 \mu s$ . The erfi and Si fits are valid up to about  $23 \mu s$  before  
 313 they completely break down. The triangular fit we can see has an E-field difference of about 200 ppb by  $30 \mu s$   
 314 which is due to the large statistical uncertainty of the Monte Carlo simulation for this large value of  $t_s$ .

315 This means that all of the fit functions are valid for  $t_s$  of up to almost  $10 \mu s$  for a realistic Monte Carlo  
 316 allowing the beam-line positron contamination of the muon beam to be skipped. With higher statistics and  
 317 using the full Fourier method, the triangular frequency distribution may be fitted to the background all the  
 318 way up to  $30 \mu s$  allowing us to skip scraping entirely. We can confidently recover the frequency distribution for  
 319  $t_s = 25 \mu s$  and the effects of scraping is probably negligible between 25 and  $30 \mu s$  since there is more scraping  
 320 in the beginning of the fast rotation signal.

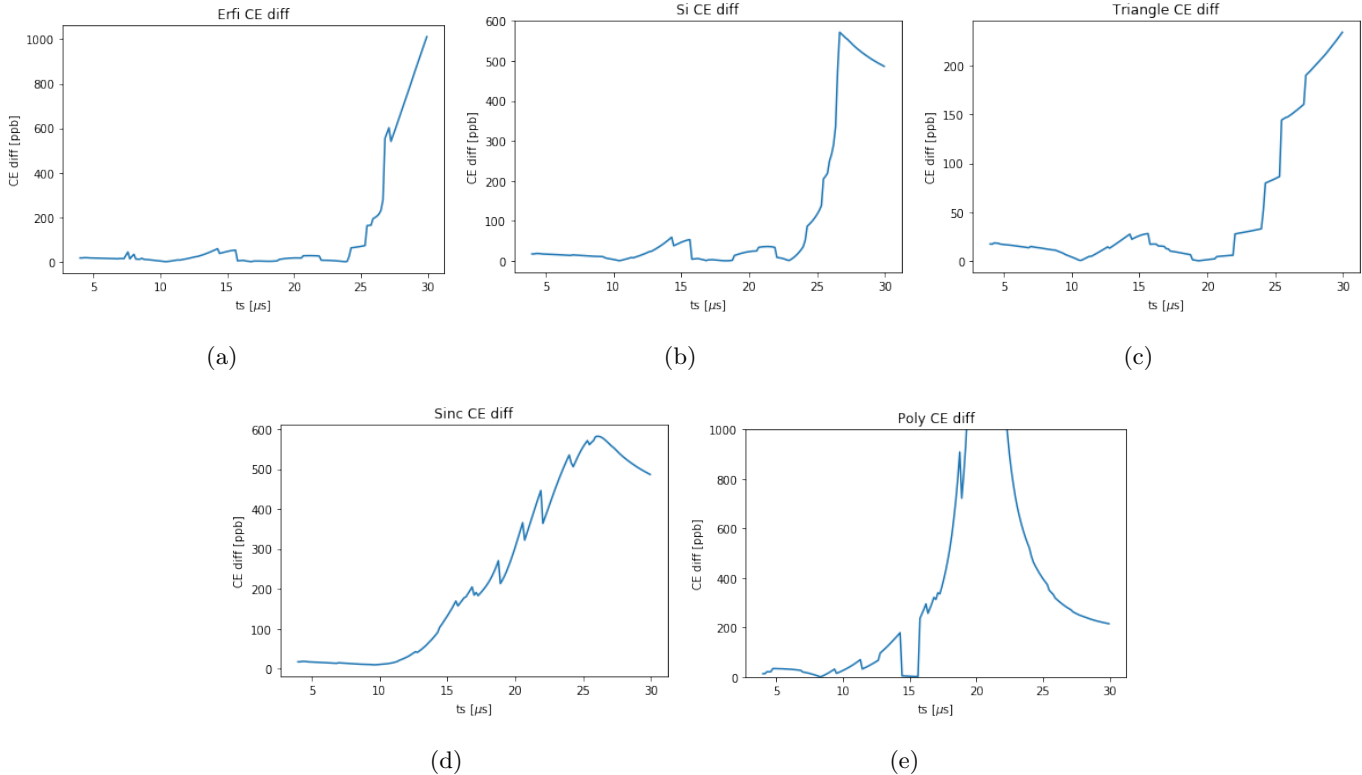


Figure 31: The difference in the recovered and actual E-field correction vs start time. Five different fit functions are used: (a) erfi, (b) Si, (c) triangle, (d) sinc, (e) poly.

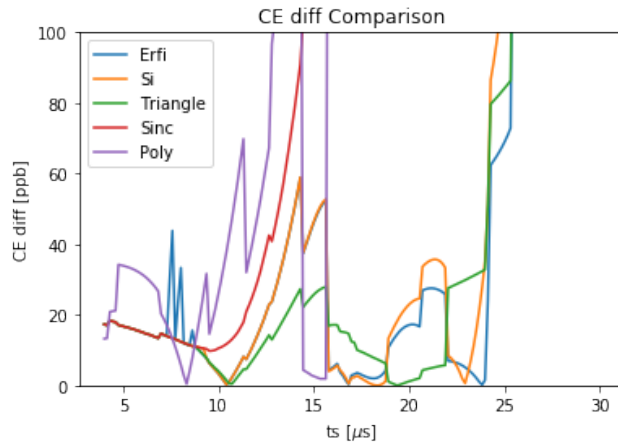


Figure 32: The difference in the recovered and actual E-field correction vs start time with all 5 different fitting functions.

## 321 6 Conclusion of background fit method

322 We derived the analytic form of the frequency background for delta function, step function, Gaussian, and  
 323 triangular frequency distributions, and we used these equations to fit the background and subtract it from the  
 324 cosine Fourier transformation to obtain the corrected frequency distribution. Using the analytic form of the  
 325 Gaussian, we were able to correct for the missing time all the way up to  $t_s = 30 \mu s$  for a Monte Carlo fast  
 326 rotation signal with Gaussian frequency distribution succeeding in the goal of skipping scraping.

327 When we use a more realistic asymmetric frequency distribution with statistical fluctuations for the Monte  
 328 Carlo, we were able to use the analytic form of a triangular frequency distribution to fit the background decently  
 329 all the way up to  $t_s = 30 \mu s$ . At this late start time the frequency distribution cannot be accurately recovered  
 330 still mostly because of the statistical uncertainty of the Monte Carlo fast rotation signal. We can confidently  
 331 confidently recover the frequency distributions values of  $t_s$  as large as  $25 \mu s$  allowing us to skip almost all of  
 332 scraping since scraping is probably negligible between 25 and  $30 \mu s$ .

333 To see the background being fitted using the full Fourier method [1] including estimations of statistical and  
 334 systematic uncertainty on real data sets refer to [6],[7],[8],[9], and Monte Carlo data sets [10]. When we use the  
 335 full Fourier method we are able to fit the background even more accurately.

## 336 7 Integral approach to the frequency background

337 We showed in previous sections that the frequency background can removed by fitting for the background and  
 338 then subtracting it out to obtain the real frequency distribution. An alternative approach to this method is to  
 339 directly calculate the background by plugging the frequency into equation (2).

### 340 7.1 Lifting the frequency distribution

341 This method is what is used by [5]. The dilemma with this approach is that to calculate the background, we  
 342 must know the complete frequency distribution, and our goal is to find the complete frequency distribution in  
 343 the first place. We get around this by using an approximate frequency distribution to plug into our background

344 equation. We take the normalization of the background to be arbitrary, and we also add an additive term to  
 345 get the following form for the background:

$$\Delta(\omega) = A \int_{\omega^-}^{\omega^+} \tilde{S}(\omega') \frac{\sin[(\omega - \omega')(t_s - t_0)]}{\omega - \omega'} d\omega' + B, \quad (25)$$

346 where we optimize the parameters A and B to fit the background. The additive term B will end up being  
 347 very small and we only include it since it is used in [5]. Since we do not have the real frequency distribution,  
 348  $\tilde{S}(\omega)$  is an approximate frequency distribution. The approximate frequency distribution is chosen by looking  
 349 at the two minima of the cosine Fourier transformation which will be located on each side of the maximum of  
 350 the cosine Fourier transformation. The values which are between the minima are considered to be the signal,  
 351 so we take the average of the minima's bin contents and then add this to the cosine Fourier transformation in  
 352 order to lift the distribution up to the x-axis. All points outside the minima are set to 0. This works for small  
 353 values of  $t_s$  when the signal is much larger than the background, however we know that for large values of  $t_s$   
 354 the signal and background completely merge.

355 Figure 33 (a) shows the cosine Fourier transform with vertical lines at the minima. The cosine Fourier  
 356 transformation is lifted up to the x-axis and the frequency bins outside the minima set to zero which is shown in  
 357 figure 33 (b). The background is calculated numerically using equation (25) with  $\tilde{S}(\omega)$  being the approximated  
 358 frequency distribution shown in (b).

359 We see in (c) that the background of the cosine Fourier transformation fits our numerically calculated  
 360 background well for this small value of  $t_s$ . In (c) the comparison of the recovered and simulated frequency  
 361 distribution is shown. The two have only a small 3.43 ppb difference. In figure 34 we see that for  $t_s = 8 \mu s$  the  
 362 integral method no longer matches the background well and we get a E-field difference of 18.89 ppb. We can  
 363 see in (b) that part of the frequency distribution is in the negative.

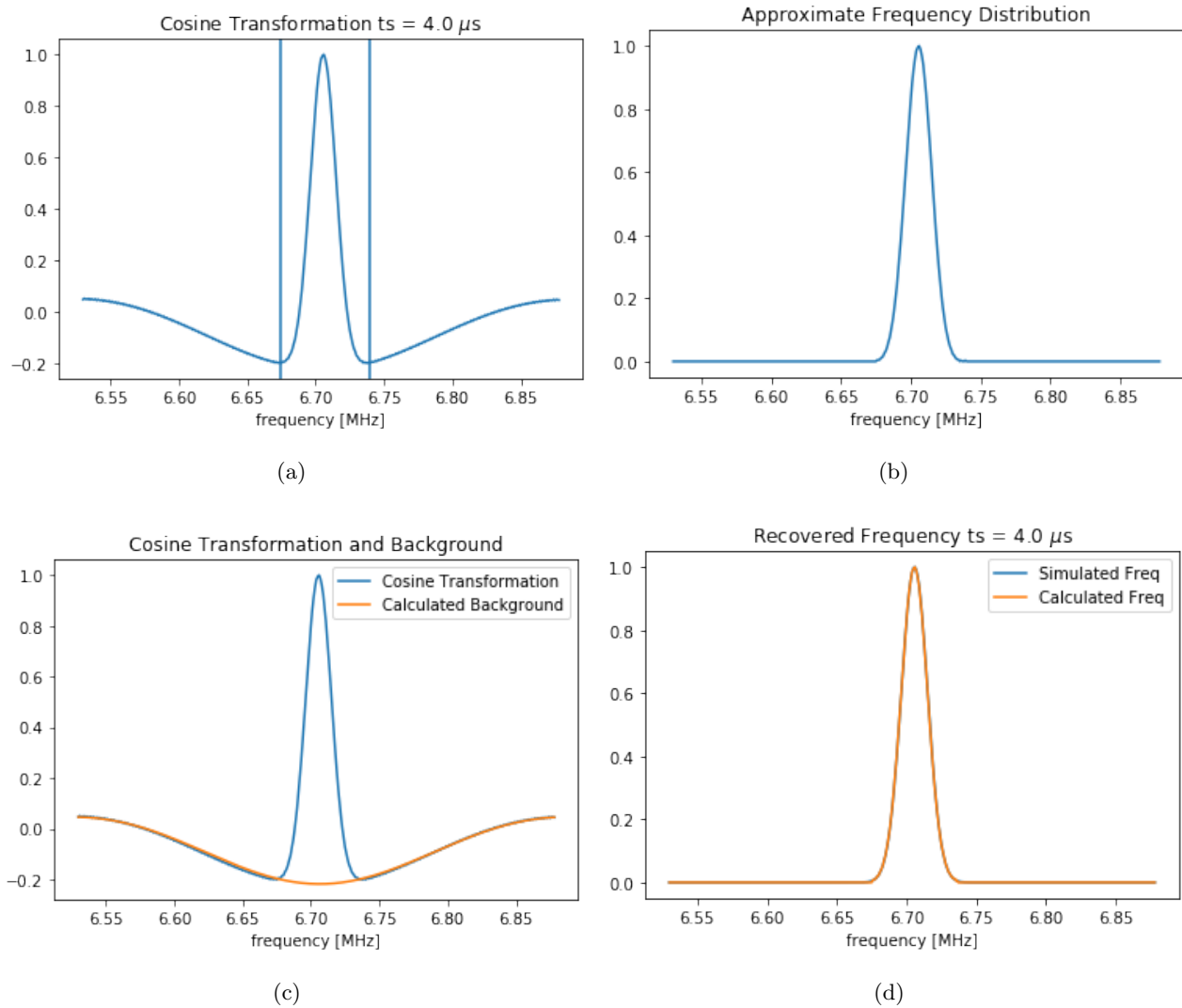


Figure 33: Integral method for  $t_s = 4 \mu s$ . (a) The cosine Fourier transformation of the fast rotation signal with the vertical lines showing the minima, (b) The approximated frequency distribution found by lifting the cosine Fourier transformation, (c) The cosine Fourier transformation with the calculated background, (d) A comparison of the recovered and simulated frequency distributions. A recovered E-field correction of -374.61 ppb and simulated value of -378.04 ppb.

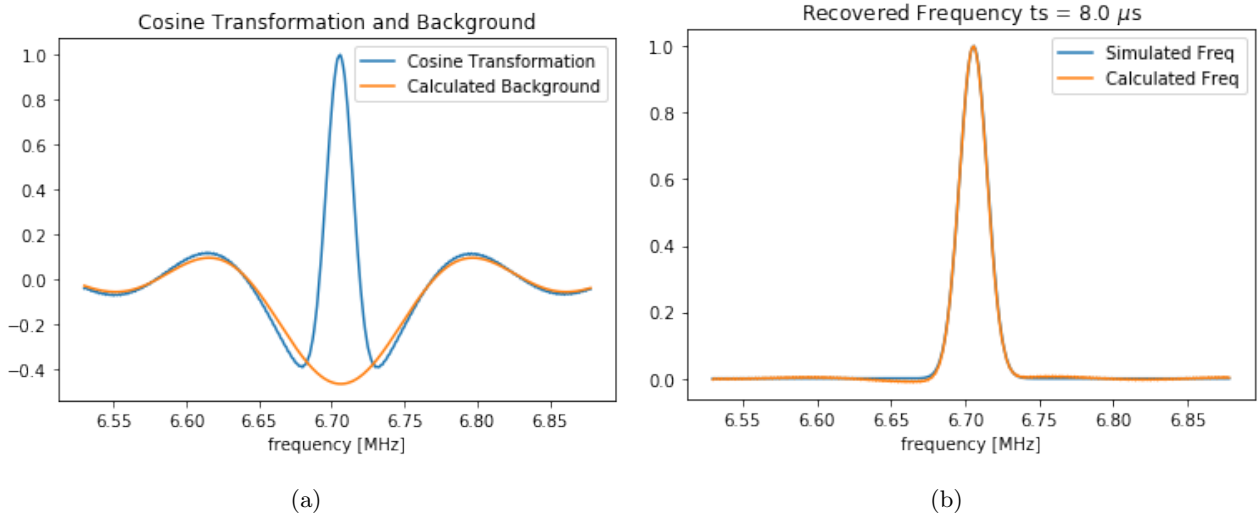


Figure 34: Integral method for  $t_s = 8 \mu s$ . (a) The cosine Fourier transformation with the calculated background, (b) A comparison of the recovered and simulated frequency distributions. A recovered E-field correction of -350.15 ppb and simulated value of -378.04 ppb.

## 364 7.2 Iteratively approximating the frequency

365 In the last section we use an approximate frequency distribution to plug into equation (25) for the background.  
 366 We can use an iterative process with each iteration using the corrected frequency distribution found in the  
 367 previous iteration as the approximate frequency distribution to plug into the equation. We always add the  
 368 correction to the original cosine Fourier transformation, and then use this to as this to calculate the background  
 369 for the next iteration.

370 We need to choose  $\tilde{S}(\omega)_0$  which is plugged in for the first iteration of the background. We could use the  
 371 same approximated frequency distribution we used in the last section by lifting the frequency distribution, but  
 372 the advantage of the iterative approach is that this is not necessary because the background is self corrective.  
 373 since the background is self corrective it does not matter much what distribution you start with. Here we  
 374 start by plugging in the actual cosine Fourier transformation in for  $\tilde{S}(\omega)_0$ , and we still recover the frequency  
 375 distribution. We then define the iterative definition of the corrected frequency distribution by:

$$\tilde{S}(\omega)_{i+1} = \tilde{S}(\omega)_0 + A_i \int_{\omega^-}^{\omega^+} \tilde{S}(\omega')_i \frac{\sin[(\omega - \omega')(t_s - t_0)]}{\omega - \omega'} d\omega' + B_i, \quad (26)$$

376 where the constants A and B are optimized for each iteration. In figure 35 we show the first two iterations  
 377 for calculating the background. For just one iteration when we use the cosine Fourier transformation as the  
 378 approximate frequency distribution to calculate the background, we get a recovered  $C_E = -384.03$  ppb compared  
 379 to the actual  $C_E = -378.04$  ppb which is 5.99 ppb apart. For iteration two we get a recovered  $C_E = -379.22$  ppb  
 380 which is only 1.18 ppb away from the actual  $C_E$ . For small values of  $t_s$  the iterative process converges after  
 381 only 3 iterations. This can be seen in figure 36 where we show the difference in  $C_E$  between the recovered and  
 382 actual frequency distributions. After only 3 iterations the  $C_E$  difference is flat as the frequency distribution  
 383 converges to a value.

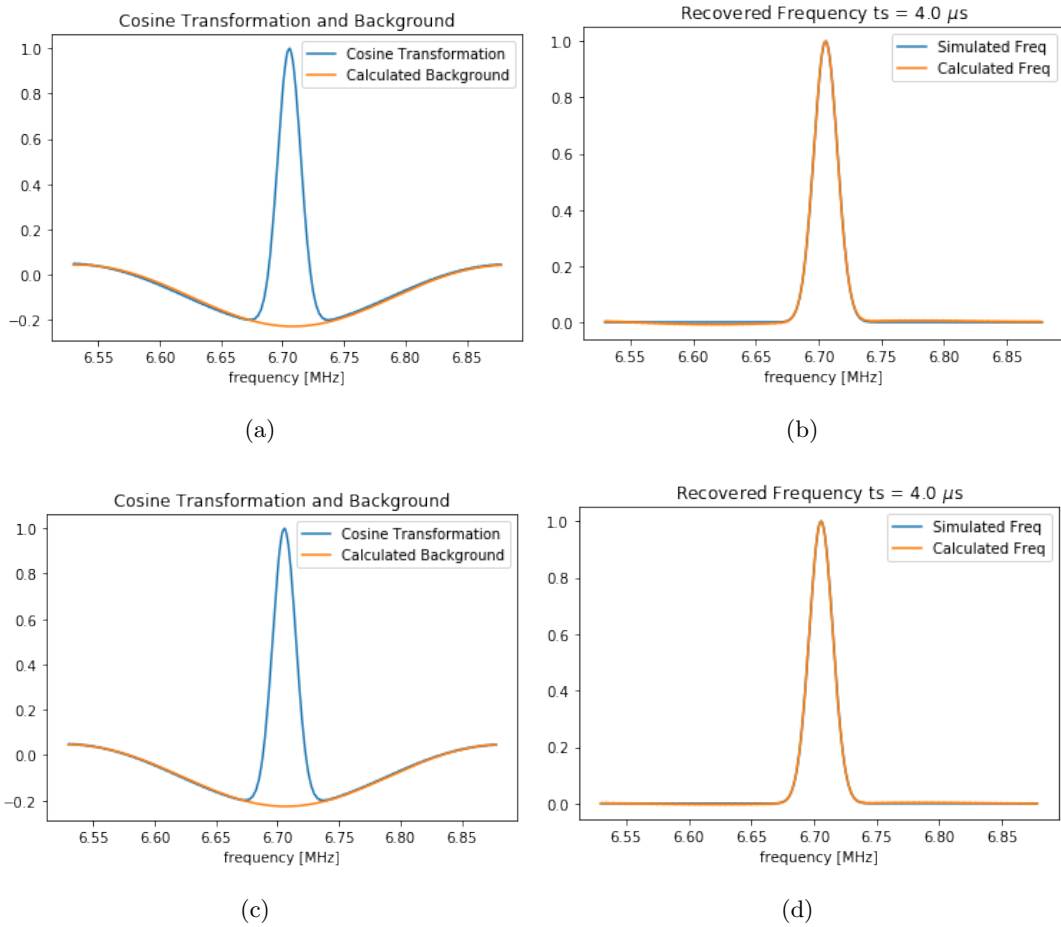


Figure 35: Iterative integral method for  $t_s = 4 \mu s$ . We start with the cosine Fourier transformation as an approximate frequency distribution to find the background. Then each iteration is used as the next approximate frequency distribution for calculating the background. (a) The cosine Fourier transformation and the calculated background for iteration 1, (b) A comparison of the recovered and simulated frequency distributions for iteration 1, (c) The cosine Fourier transformation and the calculated background for iteration 2, (d) A comparison of the recovered and simulated frequency distributions for iteration 2.

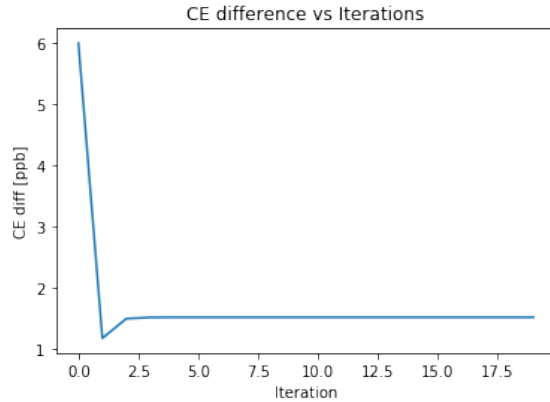


Figure 36: This is the difference between the actual and recovered E-field correction for each iteration using the iterative integral method with  $t_s = 4 \mu s$ . The  $C_E$  difference flattens after only a couple of iterations showing the convergence of the frequency distribution.

384 For larger values of  $t_s$  we need more iterations to get an accurate background. Figure 37 shows the cosine  
 385 Fourier transformation and the calculated background for the first 4 iterations of the background calculation.  
 386 For large values of  $t_s$ , the first two iterations of the background do not match the background much at all, but  
 387 by the fourth iteration our calculated background has begun to converge close to the actual background of the  
 388 cosine Fourier transformation. In figure 38 the background is shown after 100 iterations, and the calculated  
 389 background is very close to the cosine Fourier transformation background. There is no disadvantage to using  
 390 more iterations so 100 iterations are used even though the background converged long before 100 iterations.

391 Despite our fit looking decent, the frequency distribution is not exactly recovered since it is slightly lopsided.  
 392 We get a recovered  $C_E = -341.98$  ppb which is 36.06 ppb away from the actual E-field correction. If we compare  
 393 the background we get in figure 38 (a) to the background obtained in figure 34 (a) we see that the background  
 394 for the iterative method is much closer to the cosine Fourier transformation, although the recovered frequency  
 395 distributions are similarly off. In figure 39 we show how the  $C_E$  difference does not change after just 5 iterations.

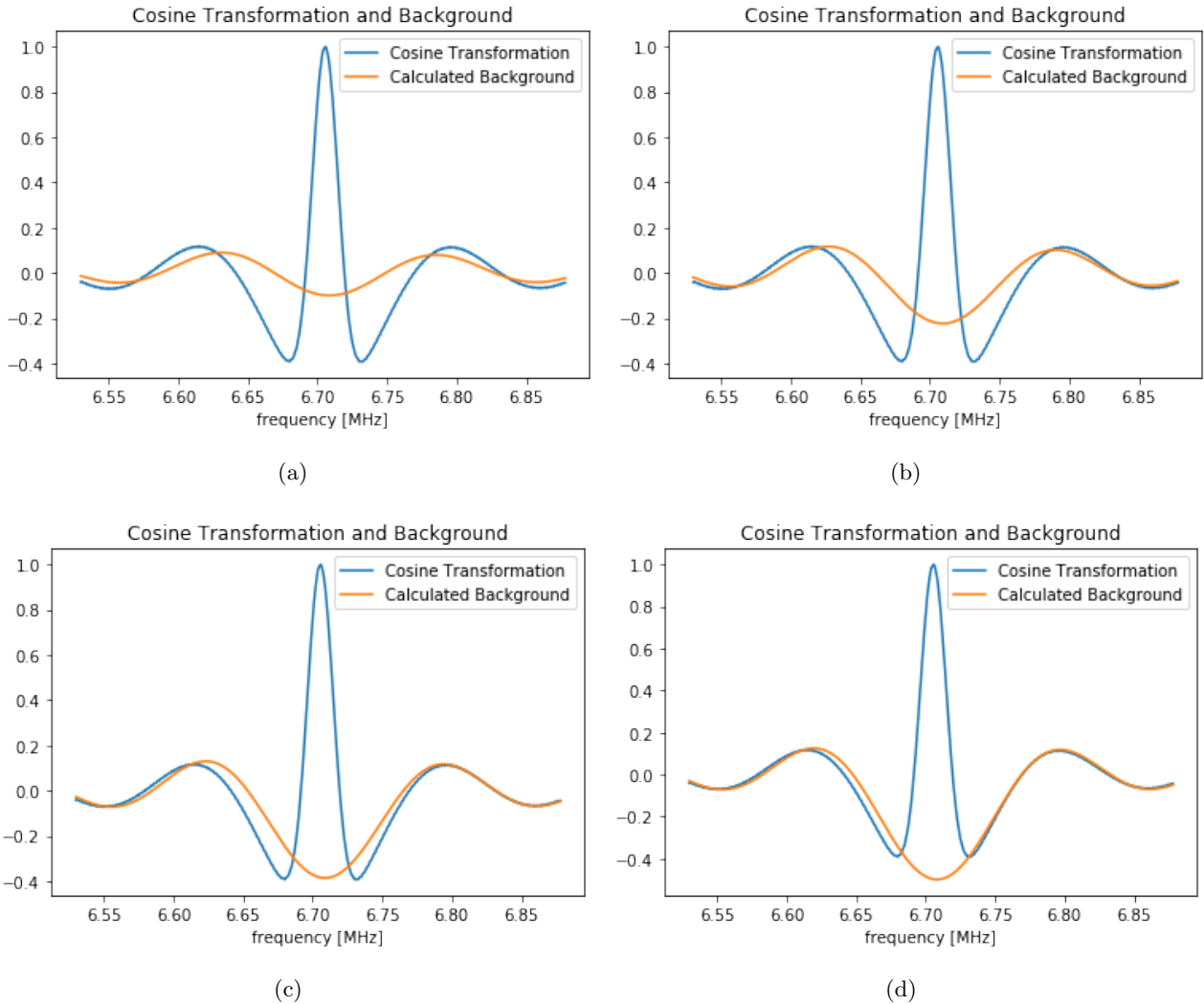


Figure 37: This is the cosine Fourier transformation and the calculated background for the iterative integral method with  $t_s = 8 \mu s$ . Four iterations are shown: (a) Iteration 1, (b) Iteration 2, (c) Iteration 3, (d) Iteration 4.

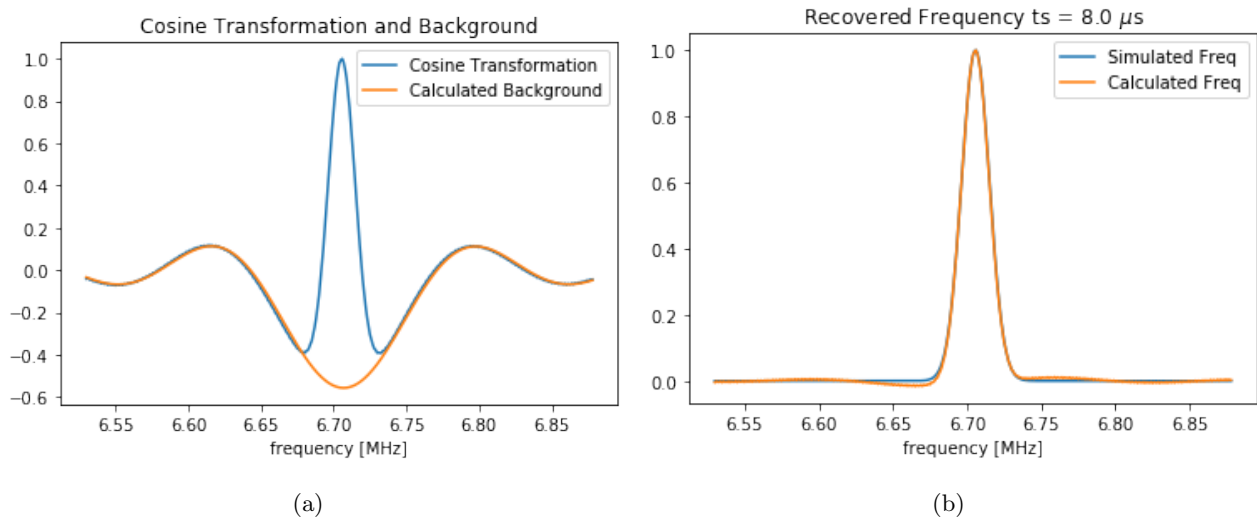


Figure 38: This is the cosine Fourier transformation and the calculated background for the iterative integral method with  $t_s = 8 \mu s$  after 100 iterations. (a) The cosine Fourier transformation and the calculated background, (b) A comparison of the recovered and simulated frequency distributions.

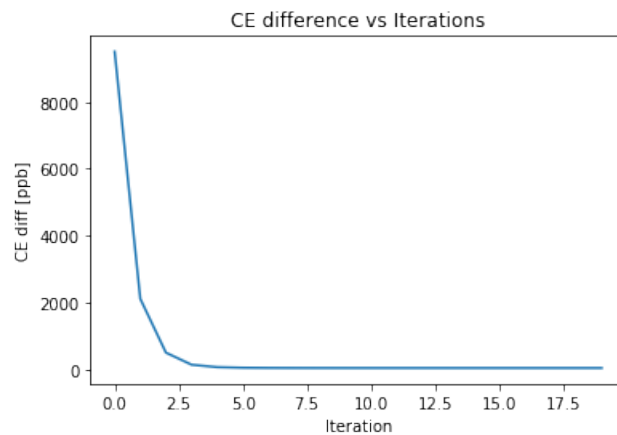


Figure 39: This is the difference between the actual and recovered E-field correction for each iteration using the iterative integral method with  $t_s = 8 \mu s$ .

## 396 8 Conclusion of integration method

397 The integral approach is not as effective as fitting the background to the cosine Fourier transformation since it  
 398 relies on knowledge of the frequency distribution. The goal when fitting for the background is to use a general  
 399 enough analytic form so that the background can be fitted regardless of the form of the frequency distribution.  
 400 The integral method is not as general since we have to figure out the form of the frequency distribution in order  
 401 to make the correction.

402 We could improve this method by using the recover the frequency distribution for  $t_s = 4 \mu s$ , and then use  
 403 this as the approximate frequency distribution for higher values of  $t_s$ . The iterative approach would still fail,  
 404 however for large values of  $t_s$ .

405 It is possible the integral method could be developed to a point where it can compete with the fit method,

406 but as it currently stands it cannot be used to skip scraping. The integral method can still be useful however  
 407 since it can use this method in conjunction with the fit method for  $t_s = 4 \mu s$  as a way of checking that the  
 408 background is properly eliminated for real data when we the real frequency distribution is unknown, and then  
 409 use difference in the recovered E-field correction between the two methods can be considered a systematic  
 410 uncertainty of the Fourier method.

## 411 Appendices

### 412 A When is $t_s$ small?

413 We consider  $t_s$  to be small when we can Taylor expand the sin function in (3). This is possible when  
 414  $|(t_s - t_0)(\omega - \omega')| \ll 1$ . The  $\omega - \omega'$  is only relevant where the frequency distribution  $\tilde{S}(\omega)$  is non-zero so  
 415 this is approximately when the frequency is within a few standard deviations from the frequency distribution.  
 416 If we assume that the full 5 standard deviation frequency distribution is confined within the collimator aperture,  
 417 then  $t_s$  is small when  $5(t_s - t_0)\sigma \ll 1$ . Values of  $t_0$  are much smaller than  $t_s$  since  $t_0$  is between 0 and 150 ns  
 418 while  $t_s$  will be at least  $4 \mu s$ , so we define  $t_s$  to be small explicitly when  $5t_s\sigma \ll 1$ . This makes it so that we  
 419 the background can be fitted for higher values of  $t_s$  when the frequency distribution has smaller width.

420 For small enough values of  $t_s$ , the background is approximately a parabola. We can see this in figure 40  
 421 where we show the background for a Gaussian frequency distribution for a value of  $t_s = 4 \mu s$ . We show explicitly  
 422 in section 4.1 that the we can Taylor expand the background itself for small values of  $t_s$ . Other forms of the  
 423 frequency background require less approximations to be made so we can use much higher values of  $t_s$  than  $4 \mu s$ .

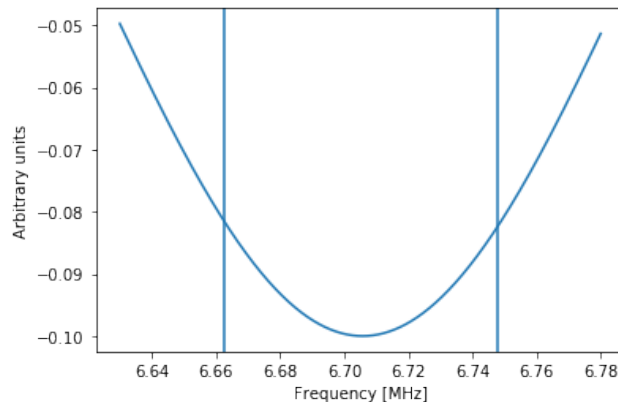


Figure 40: Frequency background from a Gaussian frequency distribution with  $t_0 = 0 \mu s$  and  $t_s = 4 \mu s$ . The vertical lines are the bounds of the collimator aperture. For this small value of  $t_s$  the background is approximately parabolic.

### 424 B Approximating the step function to be a Gaussian

425 We want to show that we can use the form of the background distribution which we found in section 2.3 and 2.2  
 426 when the frequency distribution is Gaussian or skewed Gaussian. This also includes the triangular frequency  
 427 distribution because if the step function background can be used to approximate the Gaussian background then  
 428 the triangular background can certainly do it too. This justifies what was shown visually in figure 7 that the

429 Gaussian, step function, and triangular frequency distributions all produce approximately the same background  
 430 for small values of  $t_s$ .

### 431 B.1 Gaussian frequency distribution

432 We start by Taylor expanding the Gaussian frequency distribution and plug into the equation for the correction  
 433 of the cosine Fourier transformation to show that in the limit when  $t_s$  is small the Gaussian frequency is has  
 434 the same form as the step function:

$$\tilde{S}(\omega) = \frac{1}{\sqrt{2\pi\sigma^2}} \left( 1 - \frac{(\omega - \omega_0)^2}{2\sigma^2} + \frac{(\omega - \omega_0)^4}{8\sigma^4} + \dots \right). \quad (27)$$

435 Then we can plug in the Taylor expanded series into our equation for  $\Delta(\omega)$ :

$$\begin{aligned} \Delta(\omega) &= \frac{1}{\pi} \int_{\omega^-}^{\omega^+} \frac{1}{\sqrt{2\pi\sigma^2}} \left( 1 - \frac{(\omega' - \omega_0)^2}{2\sigma^2} + \frac{(\omega' - \omega_0)^4}{8\sigma^4} + \dots \right) \frac{\sin[(\omega - \omega')(t_s - t_0)]}{\omega - \omega'} d\omega' \\ &= \frac{1}{\sqrt{2\pi^3\sigma^2}} \int_{\omega^-}^{\omega^+} \left( 1 - \frac{(\omega' - \omega_0)^2}{2\sigma^2} + \frac{(\omega' - \omega_0)^4}{8\sigma^4} + \dots \right) \frac{\sin[(\omega - \omega')(t_s - t_0)]}{\omega - \omega'} d\omega'. \end{aligned} \quad (28)$$

436 When we integrate these first terms we get:

$$\begin{aligned} \Delta(\omega) &= \frac{1}{\sqrt{2\pi^3\sigma^2}} \left[ \text{Si}((\omega - \omega^-)(t_s - t_0)) - \text{Si}((\omega - \omega^+)(t_s - t_0)) \right. \\ &\quad \left. + \frac{(\omega - \omega_0)^2}{2\sigma^2} \text{Si}((\omega - \omega^-)(t_s - t_0)) - \text{Si}((\omega - \omega^+)(t_s - t_0)) \right. \\ &\quad \left. + \frac{\sin[(\omega - \omega^-)(t_s - t_0)] + (t_s - t_0)(\omega + \omega^- - 2\omega_0) \cos[(\omega - \omega^-)(t_s - t_0)]}{2\sigma^2(t_s - t_0)^2} - \frac{\sin[(\omega - \omega^+)(t_s - t_0)] + (t_s - t_0)(\omega + \omega^+ - 2\omega_0) \cos[(\omega - \omega^+)(t_s - t_0)]}{2\sigma^2(t_s - t_0)^2} \right. \\ &\quad \left. + \frac{(\omega - \omega_0)^4}{8\sigma^4} \text{Si}((\omega - \omega^-)(t_s - t_0)) - \text{Si}((\omega - \omega^+)(t_s - t_0)) \right. \\ &\quad \left. + \frac{((t_s - t_0)^2[(6\omega_0^2 - 4\omega_0(\omega + 2\omega^-) + (\omega^2 + 2\omega^- \omega + 3\omega_-^2))] - 6) \sin[(\omega - \omega^-)(t_s - t_0)]}{8\sigma^4(t_s - t_0)^4} \right. \\ &\quad \left. - \frac{((t_s - t_0)^2[(6\omega_0^2 - 4\omega_0(\omega + 2\omega^+) + (\omega^2 + 2\omega^+ \omega + 3\omega_+^2))] - 6) \sin[(\omega - \omega^+)(t_s - t_0)]}{8\sigma^4(t_s - t_0)^4} \right. \\ &\quad \left. + \frac{(t_s - t_0)[(t_s - t_0)^2[-4\omega_0^3 + 6\omega_0(\omega + \omega^-) - 4\omega_0(\omega^2 + \omega^- \omega + \omega_-^2) + \omega^3 + \omega^- \omega^2 + \omega_-^2 \omega + \omega_-^3] - 2\omega - \omega^- + 8\omega_0] \cos[(\omega - \omega^-)(t_s - t_0)]}{8\sigma^4(t_s - t_0)^4} \right. \\ &\quad \left. - \frac{(t_s - t_0)[(t_s - t_0)^2[-4\omega_0^3 + 6\omega_0(\omega + \omega^+) - 4\omega_0(\omega^2 + \omega^+ \omega + \omega_+^2) + \omega^3 + \omega^+ \omega^2 + \omega_+^2 \omega + \omega_+^3] - 2\omega - \omega^+ + 8\omega_0] \cos[(\omega - \omega^+)(t_s - t_0)]}{8\sigma^4(t_s - t_0)^4} + \dots \right]. \end{aligned} \quad (29)$$

437 This looks like a complicated equation for the correction, but we can make some approximations to show  
 438 that the complicated sine and cosine terms are small compared to the Si terms. If we just look at the second  
 439 term in the expansion:

$$\begin{aligned}
\Delta(\omega)_2 &= \int_{\omega^-}^{\omega^+} \frac{(\omega' - \omega_0)^2 \sin[(\omega - \omega')(t_s - t_0)]}{2\sigma^2 (\omega - \omega')} d\omega' = \\
&\quad \frac{1}{2\sigma^2} [(\omega - \omega_0)^2 [\text{Si}((\omega - \omega^-)(t_s - t_0)) - \text{Si}((\omega - \omega^+)(t_s - t_0))] \\
&\quad + \frac{\sin[(\omega - \omega^-)(t_s - t_0)] + (t_s - t_0)(\omega + \omega^- - 2\omega_0) \cos[(\omega - \omega^-)(t_s - t_0)]}{(t_s - t_0)^2} \\
&\quad - \frac{\sin[(\omega - \omega^+)(t_s - t_0)] + (t_s - t_0)(\omega + \omega^+ - 2\omega_0) \cos[(\omega - \omega^+)(t_s - t_0)]}{(t_s - t_0)^2}].
\end{aligned} \tag{30}$$

440 We make the assumption that  $|(\omega - \omega^-)(t_s - t_0)|$  and  $|(\omega - \omega^+)(t_s - t_0)|$  are small quantities such that  
441 we can invoke the small angle approximation  $\sin(x) \approx x$  and  $\cos(x) \approx 1$  for  $|x| \ll 1$ . Then we can say that  
442  $\sin[(\omega - \omega^-)(t_s - t_0)] \approx (\omega - \omega^-)(t_s - t_0)$ ,  $\sin[(\omega - \omega^+)(t_s - t_0)] \approx (\omega - \omega^+)(t_s - t_0)$  and  $\cos[(\omega - \omega^-)(t_s - t_0)] \approx 1$ ,  
443  $\cos[(\omega - \omega^+)(t_s - t_0)] \approx 1$ . When we make this assumption in for  $\Delta(\omega)_2$ , the second term in the background  
444 Taylor expansion, we get the following cancellation:

$$\begin{aligned}
\Delta(\omega)_2 &= \int_{\omega^-}^{\omega^+} \frac{(\omega' - \omega_0)^2 \sin[(\omega - \omega')(t_s - t_0)]}{2\sigma^2 (\omega - \omega')} d\omega' \approx \\
&\quad \frac{1}{2\sigma^2} [(\omega - \omega_0)^2 [\text{Si}((\omega - \omega^-)(t_s - t_0)) - \text{Si}((\omega - \omega^+)(t_s - t_0))] \\
&\quad + \frac{(\omega - \omega^-)(t_s - t_0) + (t_s - t_0)(\omega + \omega^- - 2\omega_0)}{(t_s - t_0)^2} - \frac{(\omega - \omega^+)(t_s - t_0) + (t_s - t_0)(\omega + \omega^+ - 2\omega_0)}{(t_s - t_0)^2}] \\
&\quad = \frac{1}{2\sigma^2} [(\omega - \omega_0)^2 [\text{Si}((\omega - \omega^-)(t_s - t_0)) - \text{Si}((\omega - \omega^+)(t_s - t_0))] \\
&\quad + \frac{[(\omega - \omega^-) + (\omega + \omega^- - 2\omega_0)] - [(\omega - \omega^+) + (\omega + \omega^+ - 2\omega_0)]}{(t_s - t_0)}] \\
&\quad = \frac{1}{2\sigma^2} [(\omega - \omega_0)^2 [\text{Si}((\omega - \omega^-)(t_s - t_0)) - \text{Si}((\omega - \omega^+)(t_s - t_0))] + \frac{2(\omega - \omega_0) - 2(\omega - \omega_0)}{(t_s - t_0)}] \\
&\quad = \frac{(\omega - \omega_0)^2}{2\sigma^2} [\text{Si}((\omega - \omega^-)(t_s - t_0)) - \text{Si}((\omega - \omega^+)(t_s - t_0))],
\end{aligned} \tag{31}$$

445 so the sine and cosine terms have been eliminated. We also want to make sure that the Si terms do not  
446 cancel like the sine and cosine terms do under the small angle approximation. The Si function has a Taylor  
447 expansion like where  $\text{Si}(x) = x - x^3/18 + x^5/600 + \dots$ , and we can then make the approximation that  $\text{Si}(x) \approx x$   
448 for  $|x| \ll 1$ .

449 We can check now that under this approximation the Si terms does not cancel:

$$\begin{aligned}
\Delta(\omega)_2 &= \int_{\omega^-}^{\omega^+} \frac{(\omega' - \omega_0)^2}{2\sigma^2} \frac{\sin[(\omega - \omega')(t_s - t_0)]}{\omega - \omega'} d\omega' \approx \frac{(\omega - \omega_0)^2}{2\sigma^2} [\text{Si}((\omega - \omega^-)(t_s - t_0)) - \text{Si}((\omega - \omega^+)(t_s - t_0))] \\
&\approx \frac{(\omega - \omega_0)^2}{2\sigma^2} [(\omega - \omega^-)(t_s - t_0) - (\omega - \omega^+)(t_s - t_0)] \\
&= \frac{(t_s - t_0)(\omega^+ - \omega^-)(\omega - \omega_0)^2}{2\sigma^2}.
\end{aligned} \tag{32}$$

450 This term has nontrivial  $\omega$  dependence in the approximation so the Si terms cannot be left out. So in the  
451 small angle approximation we eliminate the sine and cosine terms but leave the Si function so that:

$$\begin{aligned}
\Delta(\omega) &\approx \frac{1}{\sqrt{2\pi^3\sigma^2}} [\text{Si}((\omega - \omega^-)(t_s - t_0)) - \text{Si}((\omega - \omega^+)(t_s - t_0))] \\
&\quad + \frac{(\omega - \omega_0)^2}{2\sigma^2} \text{Si}((\omega - \omega^-)(t_s - t_0)) - \text{Si}((\omega - \omega^+)(t_s - t_0)) \\
&\quad + \frac{(\omega - \omega_0)^4}{8\sigma^4} \text{Si}((\omega - \omega^-)(t_s - t_0)) - \text{Si}((\omega - \omega^+)(t_s - t_0)) + \dots].
\end{aligned} \tag{33}$$

452 When we group the Si terms together we get:

$$\Delta(\omega) = \frac{1}{\sqrt{2\pi^3\sigma^2}} \left(1 - \frac{(\omega - \omega_0)^2}{2\sigma^2} + \frac{(\omega - \omega_0)^4}{8\sigma^4} + \dots\right) [\text{Si}((\omega - \omega^-)(t_s - t_0)) - \text{Si}((\omega - \omega^+)(t_s - t_0))], \tag{34}$$

453 and we have recovered the Taylor series for the Gaussian so we can restore our original signal:

$$\Delta(\omega) = \frac{1}{\sqrt{2\pi^3\sigma^2}} e^{-\frac{(\omega - \omega_0)^2}{2\sigma^2}} [\text{Si}((\omega - \omega^-)(t_s - t_0)) - \text{Si}((\omega - \omega^+)(t_s - t_0))]. \tag{35}$$

454 We have shown that for a frequency distribution  $\tilde{S}(\omega)$  which is Gaussian, we the correction take the following  
455 approximate form:

$$\Delta(\omega) = \frac{1}{\pi} \int_{\omega^-}^{\omega^+} \tilde{S}(\omega') \frac{\sin[(\omega - \omega')(t_s - t_0)]}{\omega - \omega'} d\omega' \approx \frac{1}{\pi} \tilde{S}(\omega) [\text{Si}((\omega - \omega^-)(t_s - t_0)) - \text{Si}((\omega - \omega^+)(t_s - t_0))]. \tag{36}$$

456 This is the same form as when we used a step function as our frequency distribution, since if we plugged  
457 in the step function in equation 7 in for  $\tilde{S}(\omega)$  then we would recover the exact equation (22) for the frequency  
458 background found using the step function. This means we can use the step function approximation of the  
459 frequency distribution to fit the frequency background even for the Gaussian frequency distribution.

## 460 B.2 Skewed Gaussian frequency distribution

461 We can now try using a skewed Gaussian so that we do not have an even frequency distribution If we assume  
462 a skewed Gaussian frequency distribution centered at the magic frequency  $\omega_0$  with a standard deviation  $\sigma$  and  
463 now we define the skew of the Gaussian as  $\alpha$ :

$$\tilde{S}(\omega) = \frac{1}{\sqrt{2\pi\sigma^2}} e^{-\frac{(\omega-\omega_0)^2}{2\sigma^2}} [1 + \operatorname{erf}(\frac{\alpha(\omega-\omega_0)}{\sqrt{2}\sigma})]. \quad (37)$$

464 Then we plug into the equation for the correction to the cosine Fourier transformation:

$$\begin{aligned} \Delta(\omega) &= \frac{1}{\pi} \int_{\omega^-}^{\omega^+} \tilde{S}(\omega') \frac{\sin[(\omega-\omega')(t_s-t_0)]}{\omega-\omega'} d\omega' = \frac{1}{\sqrt{2\pi^3\sigma^2}} \int_{\omega^-}^{\omega^+} e^{-\frac{(\omega'-\omega_0)^2}{2\sigma^2}} [1 + \operatorname{erf}(\frac{\alpha(\omega'-\omega_0)}{\sqrt{2}\sigma})] \frac{\sin[(\omega-\omega')(t_s-t_0)]}{\omega-\omega'} d\omega' \\ &= \frac{1}{\sqrt{2\pi^3\sigma^2}} \left[ \int_{\omega^-}^{\omega^+} e^{-\frac{(\omega'-\omega_0)^2}{2\sigma^2}} \frac{\sin[(\omega-\omega')(t_s-t_0)]}{\omega-\omega'} d\omega' + \int_{\omega^-}^{\omega^+} e^{-\frac{(\omega'-\omega_0)^2}{2\sigma^2}} \operatorname{erf}(\frac{\alpha(\omega'-\omega_0)}{\sqrt{2}\sigma}) \frac{\sin[(\omega-\omega')(t_s-t_0)]}{\omega-\omega'} d\omega' \right]. \end{aligned} \quad (38)$$

465 The first term we get is exactly the same term we solved for in the case of the Gaussian frequency distribution  
466 with our earlier approximation so we already know the answer to that and can plug in:

$$\begin{aligned} \Delta(\omega) &\approx \frac{1}{\sqrt{2\pi^3\sigma^2}} \left[ e^{-\frac{(\omega-\omega_0)^2}{2\sigma^2}} [\operatorname{Si}((\omega-\omega^-)(t_s-t_0)) - \operatorname{Si}((\omega-\omega^+)(t_s-t_0))] \right. \\ &\quad \left. + \int_{\omega^-}^{\omega^+} e^{-\frac{(\omega'-\omega_0)^2}{2\sigma^2}} \operatorname{erf}(\frac{\alpha(\omega'-\omega_0)}{\sqrt{2}\sigma}) \frac{\sin[(\omega-\omega')(t_s-t_0)]}{\omega-\omega'} d\omega' \right] \end{aligned} \quad (39)$$

467 We can try and figure out what the second term by assuming that the erf function is small. The Taylor  
468 expansion of the erf function is as follows:

$$\operatorname{erf}(x) = \frac{2}{\sqrt{\pi}} \sum_{n=0}^{\infty} \frac{(-1)^n x^{2n+1}}{n!(2n+1)} = \frac{2}{\sqrt{\pi}} \left( x - \frac{x^3}{3} + \frac{x^5}{10} - \frac{x^7}{42} + \dots \right), \quad (40)$$

469 and since  $\omega'$  is bounded  $\omega^- \leq \omega' \leq \omega^+$ , we can say that the argument of the erf function  $\frac{\alpha(\omega'-\omega_0)}{\sqrt{2}\sigma}$  is small  
470 for small  $\alpha$ . Therefore, when  $\frac{(\omega'-\omega_0)}{\sigma} \sim 1$  and  $|\alpha| \ll 1$  we can make the approximation that:

$$\operatorname{erf}\left[\frac{\alpha(\omega'-\omega_0)}{\sqrt{2}\sigma}\right] \approx \sqrt{\frac{2}{\pi}} \frac{\alpha(\omega'-\omega_0)}{\sigma}. \quad (41)$$

471 In this small skewness limit, we can plug this approximation into the equation for the correction:

$$\begin{aligned} \Delta(\omega) &\approx \frac{1}{\sqrt{2\pi^3\sigma^2}} \left[ e^{-\frac{(\omega-\omega_0)^2}{2\sigma^2}} [\operatorname{Si}((\omega-\omega^-)(t_s-t_0)) - \operatorname{Si}((\omega-\omega^+)(t_s-t_0))] \right. \\ &\quad \left. + \int_{\omega^-}^{\omega^+} e^{-\frac{(\omega'-\omega_0)^2}{2\sigma^2}} \sqrt{\frac{2}{\pi}} \frac{\alpha(\omega'-\omega_0)}{\sigma} \frac{\sin[(\omega-\omega')(t_s-t_0)]}{\omega-\omega'} d\omega' \right] \\ &\approx \frac{1}{\sqrt{2\pi^3\sigma^2}} e^{-\frac{(\omega-\omega_0)^2}{2\sigma^2}} [\operatorname{Si}((\omega-\omega^-)(t_s-t_0)) - \operatorname{Si}((\omega-\omega^+)(t_s-t_0))] \\ &\quad + \frac{\alpha}{\pi^2\sigma^2} \int_{\omega^-}^{\omega^+} e^{-\frac{(\omega'-\omega_0)^2}{2\sigma^2}} (\omega'-\omega_0) \frac{\sin[(\omega-\omega')(t_s-t_0)]}{\omega-\omega'} d\omega'. \end{aligned} \quad (42)$$

We can then Taylor expand the Gaussian as we did before for the case of a Gaussian frequency distribution:

$$\begin{aligned}
\Delta(\omega) &\approx \frac{1}{\sqrt{2\pi^3\sigma^2}} e^{-\frac{(\omega'-\omega_0)^2}{2\sigma^2}} \left[ \text{Si}((\omega - \omega^-)(t_s - t_0)) - \text{Si}((\omega - \omega^+)(t_s - t_0)) \right] \\
&\quad + \frac{\alpha}{\pi^2\sigma^2} \int_{\omega^-}^{\omega^+} e^{-\frac{(\omega'-\omega_0)^2}{2\sigma^2}} (\omega' - \omega_0) \frac{\sin[(\omega - \omega')(t_s - t_0)]}{\omega - \omega'} d\omega' \\
&= \frac{1}{\sqrt{2\pi^3\sigma^2}} e^{-\frac{(\omega'-\omega_0)^2}{2\sigma^2}} \left[ \text{Si}((\omega - \omega^-)(t_s - t_0)) - \text{Si}((\omega - \omega^+)(t_s - t_0)) \right] \\
&\quad + \frac{\alpha}{\pi^2\sigma^2} \int_{\omega^-}^{\omega^+} \left( 1 - \frac{(\omega' - \omega_0)^2}{2\sigma^2} + \frac{(\omega' - \omega_0)^4}{8\sigma^4} + \dots \right) (\omega' - \omega_0) \frac{\sin[(\omega - \omega')(t_s - t_0)]}{\omega - \omega'} d\omega' \\
&= \frac{1}{\sqrt{2\pi^3\sigma^2}} e^{-\frac{(\omega'-\omega_0)^2}{2\sigma^2}} \left[ \text{Si}((\omega - \omega^-)(t_s - t_0)) - \text{Si}((\omega - \omega^+)(t_s - t_0)) \right] \\
&\quad + \frac{\alpha}{\pi^2\sigma^2} \int_{\omega^-}^{\omega^+} \left[ (\omega' - \omega_0) - \frac{(\omega' - \omega_0)^3}{2\sigma^2} + \frac{(\omega' - \omega_0)^5}{8\sigma^4} + \dots \right] \frac{\sin[(\omega - \omega')(t_s - t_0)]}{\omega - \omega'} d\omega' \\
&= \frac{1}{\sqrt{2\pi^3\sigma^2}} \left[ e^{-\frac{(\omega'-\omega_0)^2}{2\sigma^2}} \left[ \text{Si}((\omega - \omega^-)(t_s - t_0)) - \text{Si}((\omega - \omega^+)(t_s - t_0)) \right] \right. \\
&\quad + \frac{\alpha}{\pi^2\sigma^2} \left[ (\omega - \omega_0) \left[ \text{Si}((\omega - \omega^-)(t_s - t_0)) - \text{Si}((\omega - \omega^+)(t_s - t_0)) \right] + \frac{\cos[(\omega - \omega^-)(t_s - t_0)] - \cos[(\omega - \omega^+)(t_s - t_0)]}{(t_s - t_0)} \right. \\
&\quad \quad + \frac{1}{2\sigma^2} \left[ (\omega - \omega_0)^3 \left[ \text{Si}((\omega - \omega^-)(t_s - t_0)) - \text{Si}((\omega - \omega^+)(t_s - t_0)) \right] \right. \\
&\quad \quad + \frac{(\omega + 2\omega^- - 3\omega_0) \sin[(\omega - \omega^-)(t_s - t_0)]}{(t_s - t_0)^2} - \frac{(\omega + 2\omega^+ - 3\omega_0) \sin[(\omega - \omega^+)(t_s - t_0)]}{(t_s - t_0)^2} \\
&\quad \quad + \frac{((t_s - t_0)^2 [3\omega_0^2 - 3\omega_0(\omega^- + \omega) + (\omega_-^2 + \omega^- \omega + \omega^2)] - 2) \cos[(\omega - \omega^-)(t_s - t_0)]}{(t_s - t_0)^3} \\
&\quad \quad \left. \left. - \frac{((t_s - t_0)^2 [3\omega_0^2 - 3\omega_0(\omega^+ + \omega) + (\omega_+^2 + \omega^+ \omega + \omega^2)] - 2) \cos[(\omega - \omega^+)(t_s - t_0)]}{(t_s - t_0)^3} + \dots \right] \right]. \quad (43)
\end{aligned}$$

This equation for the correction looks complicated, but we can simplify the sine and cosine terms just like we did for the case of a Gaussian frequency distribution. We do this by making the assumption that  $|(\omega - \omega^+)(t_s - t_0)| \ll 1$  and  $|(\omega - \omega^-)(t_s - t_0)| \ll 1$ . Then we can make the small angle approximation in the sine and cosine function like we did before to show that the sine and cosine terms are small compared to the Si terms. If we just look at the first term:

$$\begin{aligned}
\Delta(\omega)_1 &= \frac{\alpha}{\pi^2\sigma^2} \int_{\omega^-}^{\omega^+} (\omega' - \omega_0) \frac{\sin[(\omega - \omega')(t_s - t_0)]}{\omega - \omega'} d\omega' \\
&= \frac{\alpha}{\pi^2\sigma^2} \left[ (\omega - \omega_0) \left[ \text{Si}((\omega - \omega^-)(t_s - t_0)) - \text{Si}((\omega - \omega^+)(t_s - t_0)) \right] + \frac{\cos[(\omega - \omega^-)(t_s - t_0)] - \cos[(\omega - \omega^+)(t_s - t_0)]}{(t_s - t_0)} \right]. \quad (44)
\end{aligned}$$

Then we can set  $\cos[(\omega - \omega^+)(t_s - t_0)] \approx 1$  and  $\cos[(\omega - \omega^-)(t_s - t_0)] \approx 1$  so that now:

$$\begin{aligned}
\Delta(\omega)_1 &= \frac{\alpha}{\pi^2 \sigma^2} \int_{\omega^-}^{\omega^+} \omega' \frac{\sin[(\omega - \omega')(t_s - t_0)]}{\omega - \omega'} d\omega' \\
&= \frac{\alpha}{\pi^2 \sigma^2} \left[ (\omega - \omega_0) [\text{Si}((\omega - \omega^-)(t_s - t_0)) - \text{Si}((\omega - \omega^+)(t_s - t_0))] + \frac{1 - 1}{(t_s - t_0)} \right] \\
&= \frac{\alpha}{\pi^2 \sigma^2} \left[ (\omega - \omega_0) [\text{Si}((\omega - \omega^-)(t_s - t_0)) - \text{Si}((\omega - \omega^+)(t_s - t_0))] \right].
\end{aligned} \tag{45}$$

479 The first term of the expansion will be small compared to the Si terms, so we can eliminate the sine and  
480 cosine terms. We can then restore the Gaussian from its Taylor series:

$$\begin{aligned}
\Delta(\omega) &\approx \frac{1}{\sqrt{2\pi^3\sigma^2}} e^{-\frac{(\omega' - \omega_0)^2}{2\sigma^2}} [\text{Si}((\omega - \omega^-)(t_s - t_0)) - \text{Si}((\omega - \omega^+)(t_s - t_0))] \\
&+ \frac{\alpha}{\pi^2 \sigma^2} \left[ \left( (\omega - \omega_0) - \frac{(\omega - \omega_0)^3}{2\sigma^2} + \frac{(\omega - \omega_0)^5}{8\sigma^4} + \dots \right) [\text{Si}((\omega - \omega^-)(t_s - t_0)) - \text{Si}((\omega - \omega^+)(t_s - t_0))] \right] \\
&= \frac{1}{\sqrt{2\pi^3\sigma^2}} e^{-\frac{(\omega - \omega_0)^2}{2\sigma^2}} [\text{Si}((\omega - \omega^-)(t_s - t_0)) - \text{Si}((\omega - \omega^+)(t_s - t_0))] \\
&+ \frac{\alpha}{\pi^2 \sigma^2} \left[ (\omega - \omega_0) e^{-\frac{(\omega - \omega_0)^2}{2\sigma^2}} [\text{Si}((\omega - \omega^-)(t_s - t_0)) - \text{Si}((\omega - \omega^+)(t_s - t_0))] \right] \\
&= \left( \frac{1}{\sqrt{2\pi^3\sigma^2}} + \frac{\alpha(\omega - \omega_0)}{\pi^2 \sigma^2} \right) e^{-\frac{(\omega - \omega_0)^2}{2\sigma^2}} [\text{Si}((\omega - \omega^-)(t_s - t_0)) - \text{Si}((\omega - \omega^+)(t_s - t_0))].
\end{aligned} \tag{46}$$

481 This is the form of the correction for small skewness  $|\alpha| \ll 1$ . Notice when  $\alpha = 0$  then the equation for the  
482 correction of the Gaussian is restored. We can see that we get approximately our original frequency distribution  
483 times the Si terms back because of the following:

$$\Delta(\omega) \approx \frac{1}{\pi} \left( \frac{1}{\sqrt{2\pi\sigma^2}} \left( 1 + \frac{\alpha(\omega - \omega_0)}{\sqrt{2}\sigma} \right) e^{-\frac{(\omega - \omega_0)^2}{2\sigma^2}} \right) [\text{Si}((\omega - \omega^-)(t_s - t_0)) - \text{Si}((\omega - \omega^+)(t_s - t_0))]. \tag{47}$$

484 We recognize the first part of the equation as our original frequency distribution. If we have a frequency  
485 distribution  $\tilde{S}(\omega)$  which is some Gaussian distribution with a small amount of skewness, then we can expect to  
486 get a correction of approximately proportional to the distribution. This matches the results of what we got for  
487 the case when  $\tilde{S}(\omega)$  is a pure Gaussian:

$$\Delta(\omega) = \frac{1}{\pi} \int_{\omega^-}^{\omega^+} \tilde{S}(\omega') \frac{\sin[(\omega - \omega')(t_s - t_0)]}{\omega - \omega'} d\omega' \approx \frac{1}{\pi} \tilde{S}(\omega) [\text{Si}((\omega - \omega^-)(t_s - t_0)) - \text{Si}((\omega - \omega^+)(t_s - t_0))], \tag{48}$$

488 for  $|(\omega - \omega^+)(t_s - t_0)| \ll 1$  and  $|(\omega - \omega^-)(t_s - t_0)| \ll 1$  with skewness  $|\alpha| \ll 1$ . Like we said for the Gaussian  
489 frequency distribution if we make the frequency distribution into a step function with some bounds within  
490 the collimator aperture, then we recovered the exact result of the background for the step function frequency  
491 distribution. This means that even for a slightly skewed Gaussian distribution we can use the Si functions to  
492 approximate the background. since we know the step function and Gaussian backgrounds are almost the same,  
493 we can also know that a Gaussian frequency background can be used for a slightly skewed Gaussian for small  
494 start times.

495 The triangular fitting function will work better for a skew Gaussian because the triangular frequency  
 496 distribution can be asymmetric so we do not have to make the assumption that  $|\alpha| \ll 1$ . This is why the  
 497 step function, Gaussian, and triangle frequency distributions all yield equivalent fitting for an asymmetric  
 498 frequency distribution up to about 20  $\mu\text{s}$  after which the approximation breaks down and the triangle frequency  
 499 distribution is superior since it relies does not rely on the assumption that  $|\alpha| \ll 1$ .

## 500 C Approximating the step function to be a Dirac delta function

501 The background for a delta function frequency distribution is the same as the other frequency distributions for  
 502 small values of  $t_s$  shown in figure 7. In the last appendix B we showed that we could use the Gaussian and  
 503 Step function backgrounds to either a Gaussian or skew-Gaussian frequency distribution when  $t_s$  is small.

504 Here we will show that the step function and the delta function frequency distributions also has the same  
 505 approximate form when  $t_s$  is small. This is not surprising since the delta function is a step function with infinite  
 506 high and infinitely small width. We also showed that the step function, Gaussian, and triangle functions are  
 507 all similar, so in the limit where the frequency distribution is approximately symmetric and  $t_s$  is small, all of  
 508 the fit functions used are approximately equivalent.

### 509 C.1 Spherical Bessel function

510 We can approximate the Si function as a sum of spherical Bessel functions [11]:

$$\text{Si}(2x) = 2x \sum_{n=0}^{\infty} [j_n(x)]^2, \quad (49)$$

511 where  $j_n$  is the nth spherical Bessel function defined by the following:

$$j_n(x) = (-x)^n \left( \frac{1}{x} \frac{d}{dx} \right)^n \frac{\sin(x)}{x}. \quad (50)$$

512 The first three spherical Bessel functions of the first kind will be the following:

$$j_0 = \frac{\sin(x)}{x} \quad (51)$$

$$j_1 = \frac{\sin(x)}{x^2} - \frac{\cos(x)}{x} \quad (52)$$

$$j_2 = \left( \frac{3}{x^3} - 1 \right) \frac{\sin(x)}{x} - \frac{3 \cos(x)}{x^2}. \quad (53)$$

$$(54)$$

513 With the assumption that our argument of the Si function  $|(\omega - \omega^+)(t_s - t_0)| \ll 1$  and  $|(\omega - \omega^-)(t_s - t_0)| \ll 1$   
 514 then we can approximate the summation to only include the first spherical Bessel function  $j_0$  such that:

$$\text{Si}(x) \approx x j_0(x/2)^2 = x \text{sinc}(x/2)^2 = 2 \sin(x/2) \text{sinc}(x/2). \quad (55)$$

515 **C.2 sinc background approximation**

516 We can plug in this the approximation in equation (55) into our approximate equation for the background with  
 517 Gaussian frequency distribution (36):

$$\begin{aligned} \Delta(\omega) &= \frac{1}{\pi} \int_{\omega^-}^{\omega^+} \tilde{S}(\omega') \frac{\sin[(\omega - \omega')(t_s - t_0)]}{\omega - \omega'} d\omega' \approx \frac{1}{\pi} \tilde{S}(\omega) [\text{Si}((\omega - \omega^-)(t_s - t_0)) - \text{Si}((\omega - \omega^+)(t_s - t_0))] \\ &\approx \frac{-2}{\pi} \tilde{S}(\omega) \left[ \sin\left[\frac{(\omega - \omega^+)(t_s - t_0)}{2}\right] \text{sinc}\left[\frac{(\omega - \omega^+)(t_s - t_0)}{2}\right] - \sin\left[\frac{(\omega - \omega^-)(t_s - t_0)}{2}\right] \text{sinc}\left[\frac{(\omega - \omega^-)(t_s - t_0)}{2}\right] \right]. \end{aligned} \quad (56)$$

518 We can see that the correction term is proportional to a sinc but we can further simplify to:

$$\begin{aligned} \Delta(\omega) &= \frac{1}{\pi} \int_{\omega^-}^{\omega^+} \tilde{S}(\omega') \frac{\sin[(\omega - \omega')(t_s - t_0)]}{\omega - \omega'} d\omega' \approx \frac{1}{\pi} \tilde{S}(\omega) [\text{Si}((\omega - \omega^-)(t_s - t_0)) - \text{Si}((\omega - \omega^+)(t_s - t_0))] \\ &\approx -\frac{2}{\pi} \tilde{S}(\omega) \left[ \sin\left[\frac{(\omega - \omega^+)(t_s - t_0)}{2}\right] \text{sinc}\left[\frac{(\omega - \omega^+)(t_s - t_0)}{2}\right] - \sin\left[\frac{(\omega - \omega^-)(t_s - t_0)}{2}\right] \text{sinc}\left[\frac{(\omega - \omega^-)(t_s - t_0)}{2}\right] \right]. \end{aligned} \quad (57)$$

519 Then when we use the exact form of the background of the step function frequency distribution (22):

$$\Delta(\omega) \approx \frac{1}{\pi} \frac{\sin\left[\left(\omega - \frac{(\omega^+ + \omega^-)}{2}\right)(t_s - t_0)\right]}{\left(\omega - \frac{(\omega^+ + \omega^-)}{2}\right)}. \quad (58)$$

520 We restrict the bounds from the collimator aperture  $\omega^+$  and  $\omega^-$ , to two points inside it, denoted as  $\omega_2$  and  
 521  $\omega_1$ , to get a generalized equation:

$$\Delta(\omega) \approx \frac{1}{\pi} \frac{\sin\left[\left(\omega - \frac{(\omega_2 + \omega_1)}{2}\right)(t_s - t_0)\right]}{\left(\omega - \frac{(\omega_2 + \omega_1)}{2}\right)}. \quad (59)$$

522 If our distribution is symmetric about some frequency  $\omega_0$  such that  $\frac{(\omega_2 + \omega_1)}{2} = \omega_0$  then we can rewrite the  
 523 background to explicitly show it is a sinc function:

$$\Delta(\omega) \approx \frac{1}{\pi} \frac{\sin[(\omega - \omega_0)(t_s - t_0)]}{(\omega - \omega_0)}, \quad (60)$$

524 which holds so long as  $|(\omega - \omega_0)(t_s - t_0)| \ll 1$ . We can then conclude that for sufficiently small values of  
 525  $t_s$ , we can use the sinc function to fit the background, even when the frequency distribution is Gaussian or  
 526 skew-Gaussian, since the Si functions are approximated to be the sinc function, and we showed in section B  
 527 that the Si function can be fitted to Gaussian or skew-Gaussian frequency distributions.

528 For a highly asymmetric frequency distribution, we can fit the background of the cosine Fourier transfor-  
 529 mation with a sinc function for at least the first 10  $\mu$ , and with Si and erfi function for at least 20  $\mu$ s, but  
 530 for greater values of  $t_s$  the triangle frequency distribution is superior since it does not assume the frequency  
 531 distribution is approximately symmetric.

## 532 References

- 533 [1] A. Chapelain, J. Fagin, D. Rubin, D. Seleznev, *Cornell fast rotation Fourier method*, [GM2-doc-18901](#)
- 534 [2] A. Chapelain, D. Rubin, D. Seleznev, *Extraction of the Muon Beam Frequency Distribution via the Fourier*  
535 *Analysis of the Fast Rotation Signal*, E989 note 130, [GM2-doc-9701](#)
- 536 [3] A. Chapelain, J. Fagin, D. Rubin, D. Seleznev, *Cornell fast rotation Monte Carlo method and user guide*,  
537 [GM2-doc-COMING-SOON](#)
- 538 [4] See ‘TMC #3’ in: [GM2-doc-13759](#)
- 539 [5] Y. Orlov et al., NIM A 482 (2002) 767-755.
- 540 [6] A. Chapelain, J. Fagin, D. Rubin, D. Seleznev, *Extraction of the radial distribution of the stored muon beam*  
541 *for the Run-1 60-hour data set via the the Cornell fast rotation Fourier method: estimation of the electric*  
542 *field correction to the anomalous spin precession frequency*, [GM2-doc-COMING-SOON](#)
- 543 [7] A. Chapelain, J. Fagin, D. Rubin, D. Seleznev, *Extraction of the radial distribution of the stored muon beam*  
544 *for the Run-1 9-day data set via the the Cornell fast rotation Fourier method: estimation of the electric field*  
545 *correction to the anomalous spin precession frequency*, [GM2-doc-COMING-SOON](#)
- 546 [8] A. Chapelain, J. Fagin, D. Rubin, D. Seleznev, *Extraction of the radial distribution of the stored muon beam*  
547 *for the Run-1 end game data set via the the Cornell fast rotation Fourier method: estimation of the electric*  
548 *field correction to the anomalous spin precession frequency*, [GM2-doc-COMING-SOON](#)
- 549 [9] A. Chapelain, J. Fagin, D. Rubin, D. Seleznev, *Extraction of the radial distribution of the stored muon beam*  
550 *for the Run-1 high kick data set via the the Cornell fast rotation Fourier method: estimation of the electric*  
551 *field correction to the anomalous spin precession frequency*, [GM2-doc-COMING-SOON](#)
- 552 [10] A. Chapelain, J. Fagin, D. Rubin, D. Seleznev, *Performance study of the Cornell fast rotation Fourier*  
553 *analysis with toy Monte Carlo simulations*, [GM2-doc-19132](#)
- 554 [11] Harris, F. E. *Spherical Bessel Expansions of Sine, Cosine, and Exponential Integrals* Appl. Numer. Math.  
555 34, 95-98, 2000.
- 556 [12] A. Chapelain, J. Fagin, D. Rubin, D. Seleznev, *Cornell fast rotation Fourier analysis user guide*, [GM2-](#)  
557 [doc-COMING-SOON](#)